Vol. 12(1), pp. 1-30, January-June 2021
DOI: 10.5897/JCEMS2020.0353
Articles Number: B4E8A7966131
ISSN 2141-6605

http://www.academicjournals.org/JCEMS

ACADEMIC JOURNALS

Journal of Chemical Engineering and Materials Science

Full Length Research Paper

Extraction and characterization of chitin and chitosan from *Callinectes amnicola* and *Penaeus notialis* shell wastes

Olaosebikan Abidoye Olafadehan*, Kehinde Olawale Amoo, Tolulase Olufunmilayo Ajayi and Victor Ehigimetor Bello

Department of Chemical and Petroleum Engineering, University of Lagos, 101017 Akoka, Yaba, Lagos, Nigeria.

Received 13 November 2020; Accepted 1 February 2021

In the current investigation, chitin and chitosan are extracted from *Callinectes amnicola* (crab) and *Penaeus notialis* (shrimp) shell wastes using predetermined optimization conditions. The shrimp shell produces higher chitin yield (26.08%), higher chitosan yield (16.93%) and higher degree of deacetylation (*DDA*) of 89.73% than the yields of chitin (19.36%), chitosan (13.29%) and the *DDA* from crab shell (84.20%). The Fourier Transform Infrared (FTIR) and acid-base titration methods are used to obtain % *DDA* of the optimized chitosan. Insignificant deviations between the *DDA* values from both methods are obtained. The experimental FTIR bands and standards for the refined chitosan from crab and shrimp shell wastes are in excellent agreement. The physicochemical properties of the raw precursors, extracted chitin and chitosan (raw and refined/decolorized) are equally evaluated. The extracted chitin and chitosan are characterized using analytical techniques. The implication of this study is in the current drive to produce chitin and chitosan from the underutilized shell wastes of *C. amnicola* and *P. notialis* of Nigerian sources with a high yield and a high *DDA*. In this study, the *P. notialis* shell is a better alternative source of chitin and chitosan than *C. amnicola* shell.

Key words: Extraction, characterization, Brunauer-Emmett-Teller (BET) surface area, Fourier Transform Infrared Spectroscopy (FTIR), scanning electron microscopy, transmission electron microscopy.

INTRODUCTION

Callinectes amnicola (crab) and *Penaeus notialis* (pink shrimp) are amongst the world's most significant kinds of seafood. Commercially, about 50% of the kinds of seafood are discarded as unsaleable products in the form of shell waste when being processed, cleaned-up and packaged. However, certain amounts of proteins (30-40%), calcium (II) trioxocarbonate (IV), $CaCO_3$ and tricalcium diphosphate, $Ca_3(PO_4)_2$, (30-50%), chitin (20-30%) and pigments (astaxanthin, canthaxanthin, lutein or β-carotene) are contained in the crustaceans' shells on a dry basis (Kumirska et al., 2010; Hajji et al., 2014; Nithya et al., 2014).

There are variations in these proportions from one crustacean shell to another and from season to season (Aranaz et al., 2009).

However, the next in importance to cellulose and the.

*Corresponding author. E-mail: oolafadehan@unilag.edu.ng. Tel: +234802-912-9559, +234703-014-4070.

second most important and abundant biopolysaccharide (or biopolymer) available in nature is β-(1→4) N- acetyl-D-glucosamine (chitin). It is a constituent of the carapaces, crusts, molluscs, outer skeleton of crustaceans (crabs, shrimps, krill, barnacles, lobsters, amongst others), insects, yeast and fungal cell walls (Arbia et al., 2013; Ji et al., 2012). The standard procedure for extraction of chitin from the crustacean shell wastes involves the following basic steps: washing, grinding and sieving of raw shell wastes, followed by demineralization (that is, elimination of $CaCO_3$ and $Ca_3(PO_4)_2$ in dilute acid), deproteinization (that is, protein separation in aqueous NaOH or KOH) and decolorization (pigments removal). The uses of enzymatic hydrolysis for deproteinization (Synowiecki and Al-Khateeb, 2003) and microorganisms for both demineralization and deproteinization have equally been reported (Synowiecki and Al-Khateeb, 2003; Shirai et al., 2003). Chitin can be found in different allomorphic forms, α and β, or as a combination of these two forms, known as γ-chitin, depending on the source of precursors used (Roberts, 1992). Amongst these forms, the most copious is α-chitin, which can be produced primarily from the outer skeletons of shrimps and crabs. The β- and γ-chitin can be produced from squid pens and fungi and yeast respectively (Campana-Filho et al., 2007). Moreover, the α-chitin can be obtained from β-chitin via treatment with alkaline solution and the resulting mixture water-flushed (Noishiki et al., 2003). The subsequent chemical conversion of chitin to β-(1→4) D-glucosamine (chitosan), known as deacetylation, removes partially or completely the acetyl group from it and this involves treatment of the former with solution of 40-50% concentrated sodium hydroxide at 100°C or above (No and Meyers, 1995; Galed et al., 2008). Hence, chitosan is an incompletely or completely deacetylated form of chitin. The former is a cationic amino biopolymer (Ibitoye et al., 2018), and thus possesses the capability to chemically cohere with anionic fats, lipids and bile acids (Sandford, 1992). Chitin and chitosan show resemblance in their structural form, except for the acetyl group in the former biopolymer, with the latter being the most useful derivative of chitin (No and Meyers, 1992). Using the European Chitin Society (EUCHIS) (2017) terminology, they can be identified as a result of their solubility in 0.1 M ethanoic acid with the insoluble and soluble materials being chitin and chitosan respectively. Their average molecular weights are in a million-fold. However, the average molecular weight of the chitosan found in the market or used industrially is between 3.8×10^3 and 5.0×10^5 g/mol with degree of *N*-acetylation being 0.02 - 0.40 (Ravi Kumar, 2000; Tajik et al., 2008). Dissimilar to plant fiber, chitosan has the capacity to form films, optical structural characteristics. For the past years, much attention has been focused on chitinous polymer as a promising renewable polymeric material. This is due to their extensive applications in the pharmaceutical and biomedical industries for enzyme immobilization and purification, in chemical plants for wastewater treatment, in food industries for food formulations as binding, gelling, thickening and stabilizing agent and in cosmetics and fiber industries (Morin-Crini et al., 2019; Casadidio et al., 2019; Jones and Pawlik, 2019; Knorr, 1984; Li et al., 1992; Prashanth and Tharanathan, 2007).

Several techniques to extract chitin from different sources have been published (Synowiecki and Al-Khateeb, 2003; Struszczyk, 2002; Hayes et al., 2008; Al-Sagheer et al., 2009; Al-Shahrani et al., 2018; Ibitoye et al., 2018). Moreover, over the years, various crustaceans have been used to extract chitin, and these different sources have been reported to affect the isolation of chitin and chitosan. Also, the percentage of chitin present in the source where it is found varies according to the origin of the source (Abdou et al., 2008; Muzzarelli and Peter, 1997). Accordingly, several works on the extraction and characterization of chitin and its derivatives from different origins have been reported (Cho et al., 1998; No et al., 2000; Kaya et al., 2015). Al-Sagheer et al. (2009) produced chitin and its derivative, chitosan, from Arabian Gulf crustaceans' sources to determine the protein content in chitin. Abdou et al. (2008) reported the production of chitin and its derivative from the crustacean of Egyptian origin. Yildiz et al. (2010) reported the extraction and characterization of chitin and chitosan from the Mediterranean crab. Nessa et al. (2010) developed a process for the preparation of chitin and chitosan from prawn shell waste of Khulna, Bangladesh, and evaluated the influence of deacetylation process during chitosan production on its physicochemical and functional properties. Limam et al. (2011) reported the extraction and characterization of chitin and chitosan from two species of crustacean of Tunisian origin. Equally, in the study of Nouri et al. (2016), chitosan (isolated from wastes of species of Indian white shrimp, *Penaeus indicus*, with a high functionality was produced using mild conditions (temperatures of 60, 80 and 100°C), concentration of alkaline (30, 40 and 50%) and times of 90, 195, 300 min. Despite all these reported works, literature is scanty on the extraction and characterization of chitin and chitosan from crustaceans of Nigerian origin. The sources of chitin are highly available in Nigeria and are abundant in the coastal areas of Nigeria (Amos, 2007; FAO, 2017). These materials litter the river banks and coastlines, thereby constituting environmental pollution because they are underutilised. Also, the crustacean shells are also discarded after processing in the food industry and these are valuable sources of chitin, which can be further processed into chitosan. Hence, the extraction of chitin and chitosan from the shell wastes of pink shrimp (*P. notialis*) and Lagoon crab (*C. amnicola*), both of Nigeria origin, using the chemical processes of demineralization, deproteinization and deacetylation respectively was investigated in this study since the main commercial

sources of chitin and chitosan are shrimp and crab shell wastes (Al-Sagheer et al., 2009; Rinaudo, 2006; Sudha et al., 2017). Before the extraction was done independently, the optimum conditions of the process were determined elsewhere by the authors using Box-Behnken design (BBD) of experiments and response surface methodology (Amoo et al., 2019; Olafadehan et al., 2020), robust quadratic models for predicting the yield of chitin and chitosan extraction, and the degree of deacetylation (*DDA*) of chitosan from both precursors were put forward. The isolated optimized chitin and chitosan from shrimp and crab waste shells were characterized by Proximate analysis, X-ray Diffraction (XRD), Energy Dispersive X-ray Spectroscopy (EDS), Fourier Transform Infrared Spectroscopy (FTIR), Brunauer-Emmett-Teller (BET) analysis, Transmission Electron Microscopy (TEM) and Scanning Electron Microscopy (SEM). These characterizations give very deep insights into the structural features of each polymer produced and their respective functional groups showing the order of quality for the different extracted polymers. The extraction and characterization of chitin and its derivatives from locally sourced Nigerian precursors provide an enormous economic benefit to the local sea foods industries in Nigeria and its applicability to the world at large.

METHODOLOGY

The crab (*C. amnicola*) and pink shrimp (*P. notialis*) used in this study were obtained from the University of Lagos lagoon and a local market in Lagos State, Nigeria respectively and their shells processed into powder.

Materials

Hydrochloric acid (~37%), and sodium hydroxide pellets (97%) were purchased from Fisher Scientific International Inc., USA while potassium permanganate (99.0%) and oxalic acid dihydrate, $C_2H_2O_4.2H_2O$, (99.5%) were purchased from J. T. Baker Co., USA.

Extraction of chitin

The crab (*C. amnicola*) and shrimp (*P. notialis*) tissues found loosely in and around the shell wastes were disposed of. The sole resulting shells were thoroughly scrubbed, washed, cleaned and dried. A Morphy Richards 100-W blender was used to thoroughly pulverize the resulting dried shell samples, which were passed through a 250-µm sieve, collected in plastic bags and then conserved at ambient temperature of (28±2°C) for supplemental analyses.

Demineralization

The process of extraction of chitin from the shell wastes involved demineralization with 2 - 4 M hydrochloric acid for 12-24 h at ambient temperature (28 ± 2°C) with constant agitation speed of 100 rpm at a solvent to solid ratio of 10:1 (w/v). Separation of the resulting acid-shell mixture was done by vacuum filtration and the solid washed thoroughly with distilled water until a neutral pH of 7 was achieved.

Deproteinization

The demineralized shells were deproteinized with 1.5 - 3.5 M sodium hydroxide for 1 - 3 h at (70 ± 0.5°C) with constant agitation speed of 100 rpm at a solvent to solid ratio of 15:1 (w/v). The resulting heterogeneous mixture was mixed thoroughly to form insoluble particles of chitin and subsequently separated by filtration using a vacuum pump. The precipitate was thoroughly washed with distilled water to bring down the pH to 7.0.

Decolorization

The extracted crude chitin from the treated crustacean shells was decolorized by treating the crude chitin with 10 g/L potassium tetraoxomanganate (VII), $KMnO_4$, for 1 h and then reacted with 10 g/L oxalic acid dehydrate, $C_2H_2O_4.2H_2O$ for another 1 h. The decolorized chitin was then separated via vacuum filtration and washed with distilled water until the pH = 7.0. The sample was dried in an oven at 80°C for 3 h and the dry weight of the decolorized chitin was recorded.

Deacetylation of chitin

The extracted decolorized chitin was converted to chitosan by the process of deacetylation. The chitin was immersed in 30-50% w/w concentration of sodium hydroxide solution for 1.5-4.5 h at (60-100)±0.5°C at a constant agitation speed of 100 rpm at a solvent to solid ratio of 10:1 (w/v). The mixture was separated by filtration powdered by a vacuum pump and the resulting solid matter/particles thoroughly washed with distilled water until the pH was neutral. The solid matter obtained (that is, chitosan) was then dried in a muffled oven at 80°C for 3 h and the dry weight was recorded.

Determination of the extraction yield and degree of deacetylation

The extraction yields of the derived chitin and the derived chitosan from *C. amnicola* and *P. notialis* shell wastes were calculated thus:

$$Y_c = \left(m_c / M_c\right) \times 100 \quad (1)$$

$$Y_{ch} = \left(m_{ch} / M_{ch}\right) \times 100 \quad (2)$$

where the subscripts *c* and *ch* represent chitin and chitosan respectively, Y_c and Y_{ch} are the respective % yields of the derived chitin and the derived chitosan, m_c and m_{ch} are the respective extraction weights of the derived chitin and derived chitosan, M_c and M_{ch} are the extraction weights of the derived chitin and derived chitosan, which are 25 g and 45 g respectively.

The acid-base titration method (Zhang et al., 2011) through some modifications was applied to determine the percent degree of deacetylation (*DDA*) of the derived chitosan experimentally. 0.125 g derived chitosan was weighed and dissolved in 30 mL of 0.1 M standard HCl aqueous solution; about 5-6 drops of methyl orange were added as indicator and then effectively agitated for 30 min until the chitosan-HCl mixture was completely homogeneous at ambient temperature. The resulting red chitosan solution was then

titrated with 0.1 M NaOH solution until it turned orange. The percentage degree of deacetylation (*DDA*) of chitosan was calculated using Equation 3:

$$\%\ DDA = \left(\frac{c_1 V_1 - c_2 V_2}{M \times 0.0994} \times 0.016 \right) \times 100 \quad (3)$$

where c_1 and c_2 are the respective concentrations of standard HCl and NaOH aqueous solutions (mol/L), V_1 the volume of 0.1 M HCl solution for chitosan dissolution (mL), V_2 the volume of 0.1 M NaOH solution consumed during titration (mL) and *M* the weight of derived chitosan (g). In Equation 3, 0.016 is a standard factor, that is the corresponding weight of the NH_2 group in 1 mL of standard 1 M HCl solution, which is expressed in g, and 0.0994 is the direct proportional ratio of NH_2 group by weight in the derived chitosan.

Physicochemical properties of raw precursors and extracted products

Several characterization techniques were used to determine the most relevant physicochemical properties of both raw precursors (that is, crab and pink shrimp shells), the derived chitin and derived chitosan samples extracted from these shells. The surface area, bulk density, pH, and iodine value experiments were all done on the extracted polymers to ascertain the physicochemical integrity of the produced polymers.

Surface area

The Brunauer-Emmett-Teller (BET) method is the most widely used procedure for the determination of the surface area of solid materials. This involves the use of the BET equation:

$$\frac{1}{v\left(\frac{p_0}{p} - 1\right)} = \frac{1}{v_m c} + \left(\frac{c-1}{c v_m}\right)\frac{p}{p_0} \quad (4)$$

where *p* is the partial vapour pressure of adsorbate gas (N_2) in equilibrium with the surface at a temperature of 77 K (Pa), p_0 the adsorbate gas (N_2) saturation pressure (Pa), *v* the volume of gas adsorbed at standard temperature and pressure (STP) (mL), v_m the volume of gas adsorbed at STP when an apparent monolayer is formed on the surface of the solid particle (mL) and *c* is a dimensionless constant that is related to the enthalpy of adsorption of the adsorbate gas on the sample (dimensionless).

In this study, the BET surface area of each sample was performed by the adsorption of $N_{2(g)}$ at 77 K using micrometric surface area analyzer (ASAP2010 Micrometric Inc. USA). Before the adsorption of $N_{2(g)}$, the sample was subjected to degassing for approximately 24 h at a final pressure and temperature of 133.32×10^{-4} Pa and 300°C respectively.

Bulk density

The bulk density, ρ_B, of each sample (derived chitin/derived chitosan) was obtained by measuring the volume of distilled water displaced by a known mass of the experimentally produced sample using a measuring cylinder. The apparent (or bulk) density of each sample was determined using the tapping procedure described by Ahmeda et al. (1997). A known weight of each sample of the adsorbent, after being dried in an oven at 105°C, was put into a 10-mL capacity graduated cylinder. To ensure the sample was totally settled, the base of the graduated cylinder was tapped severally on the laboratory benchtop until it was certain the sample had fully settled. The bulk density, ρ_B, of the sample was calculated using Equation 5:

$$\rho_B = W_{mat} / V_{mat} \quad (5)$$

where ρ_B is the bulk density of derived chitin/derived chitosan (g/mL), W_{mat} and V_{mat} are weight of dry sample (g) and its volume (mL) respectively.

Determination of pH

The pH of each of the samples was determined through a procedure described by Jayakumar and Chandrasekaran (2014) with some modifications. 1 g of the dried sample was weighed using a high-performance weighing scale and then transferred into a 100-mL breaker. 30 mL of freshly boiled and cooled water with the adjustment of pH to neutrality was mixed with the sample and temperature raised to boiling point. After a 10-min digestion, the hot solution was filtered while disposing of the first 2 mL of the filtrate. The remaining filtrate was then cooled to room temperature and the pH of the solution was determined using a pH meter.

Determination of iodine number

The iodine number, *I*, of a sample is defined as the milligrams of iodine adsorbed by 1 g of material when the iodine residual concentration in the filtrate is 0.02 N (0.01 mol/L) according to ASTM-D-4607 standard (ASTM, 1994), which was reapproved in 2011, and was based on a three-point isotherm. The sample was treated with 10 mL of 5% (v/v) HCl. The mixture was then boiled for 30 s and then cooled at room temperature. 100 mL of 0.1 N iodine solution was immediately added to the HCl-sample mixture and agitated for 30 s. The remaining solution was then paper-filtered and 50 mL of the filtrate was titrated with 0.1 N (0.05 mol L^{-1}) sodium thiosulphate pentahydrate ($Na_2S_2O_3.5H_2O$) solution using starch as indicator. Using logarithmic axes, the amount of iodine adsorbed per gram of adsorbent was plotted against the residual iodine concentration. When the residual equilibrium iodine concentration was not within 0.008 to 0.04 N, the procedure was repeated with a different mass of sample for each isotherm point. The iodine value/number, *I*, was estimated thus (Kim et al., 2001):

$$I = \left[(10 \times f' - K \times f) \times 12.69 \times 5\right] / W_s \quad (6)$$

where *I* is the iodine number of the sample (mg/g), f' is the concentration factor of iodine (dimensionless), *f* the concentration factor of 0.1 N sodium thiosulphate solution (dimensionless), *K* the titre volume of 0.1 N sodium thiosulphate solution (mL) and W_s the dry weight of the adsorbent (g). The factor 12.69 is the content of iodine in 1 mL of 0.1 M sodium thiosulphate (mg).

Determination of moisture content

The moisture content (MC), was determined by employing the

gravimetric method (Huthman et al., 2013). The water mass/weight of the sample was determined by drying the sample to constant weight and weighing the sample before and after drying. The water mass (or weight) in the sample was the difference between the weights of the wet and oven-dried samples. The moisture content (MC) was calculated using Equation 7:

$$\%\ MC = (W - w) \times 100 / W \quad (7)$$

where *W* and *w* are the respective weights of wet and oven-dried samples (g).

Determination of ash content

The % ash content, AC, of each sample was determined by placing 1 g of the sample into the previously weighed crucible. The crucible and its content were then placed in an electric oven at 110°C for about 4 h. The sample was heated in an electric muffle furnace at a sustained temperature of 600°C for 2 h. The ceramic crucible with its content was allowed to cool in a desiccator for 30 min (Jayakumar and Chandrasekaran, 2014; Mohanasrinivasan et al., 2014). The heating and cooling processes were then repeated until the difference between two consecutive weights was less than 1 mg and white ash was obtained. The % ash was determined using Equation 8:

$$\%\ AC = \left[\frac{W_1}{W_m \times \left(\frac{100 - X}{100} \right)} \right] \times 100 \quad (8)$$

where W_1 is the weight of residue (g), W_m the weight of the test sample (g) and *X* the % *MC* in the test sample.

Determination of protein

The protein percent of the derived samples was determined by the universally used Kjeldahl method for total nitrogen determination by sequentially adding 15 g of sodium (II) tetraoxosulphate (VI), Na_2SO_4, 1 g of copper (II) tetraoxosulphate (VI), $CuSO_4$, two selenised boiling granules and 25 mL of concentrated tetraoxosulphate (VI) acid (H_2SO_4) to each of the samples and then placed in a digestion flask. Digestion continued until the solution was almost colourless or light green and then left for at least a further 30 min. The solution was cooled and 200 mL of distilled water was cautiously added. 100 mL of 0.1 N HCl was then transferred into a 500-mL Erlenmeyer flask with 2-3 drops of an indicator and the flask placed underneath the condenser, ensuring that the condenser tip was immersed in the acidic solution. 100 mL of 50% (w/v) NaOH solution was slowly added down the side of the digestion flask to form a layer underneath the digestion mixture. The mixture was then heated until all ammonia had passed over into the standard acid. Approximately 150 mL of the mixture was collected and the distillate, which contains excess standard HCl in the distillate was titrated with NaOH standard solution. The protein content of the sample was determined through the use of Equations 9 to 11:

$$\%\ nitrogen(wet) = \left[\frac{(M_1 - M_2) \times 1.4007}{weight\ of\ sample} \right] \times 100 \quad (9)$$

$$\%\ nitrogen(dry) = \left[\frac{\%\, nitrogen(wet)}{100 - \%\, moisture} \right] \times 100 \quad (10)$$

$$\%\ protein = \%\ nitrogen \times 6.25 \quad (11)$$

where M_1 is the volume of standard HCl × normality of standard HCl, M_2 the volume of standard NaOH × normality of standard NaOH and 6.25 is the conversion factor for protein-nitrogen in fish and fish by-products.

Determination of fiber

The % fiber of each sample was determined by accurately weighing 1 g of the ground sample and adding 150 mL of 1.25% (w/v) tetraoxosulphate (VI) acid, after the sample had been preheated. The sample was allowed to boil for exactly 30 min. After boiling, the mixture was vacuum-filtered, washed thoroughly with distilled water and separated. The separated sample was then mixed with a preheated solution of 1.25% (w/v) potassium hydroxide and allowed to boil for 30 min. The mixture was filtered, washed and separated as before. The sample was then washed with 25 mL acetone with constant stirring. A constant dry weight was obtained after drying in an electric oven at 105°C for an hour. This weight represented the crude fiber plus ash content in comparison to the initial weight. The % fiber was determined using Equation 12:

$$\%\ fiber = \left(\frac{W_f - W_i}{W_i} \right) \times 100 \quad (12)$$

where W_f is the crude fiber plus ash content in comparison to initial sample weight (g) and W_i the initial sample weight (g).

Determination of carbohydrate content

The carbohydrate content of each of the samples was determined using AOAC standards (AOAC, 1990). Colorimetric methods such as the phenol-sulphuric or the anthrone procedures may be applied to assess the total amount of carbohydrates in sample materials; however, a great degree of interference is expected. Due to this general difficulty, the carbohydrate percent of materials is usually calculated by subtracting the total proximate results from 100%.

Analytical procedures

The Fourier Transform Infrared (FTIR) spectroscopy of each sample was measured on KBr/Ge mid-infrared beam-splitter discs in the transmission mode in the range 350-4400 cm^{-1} by using Nicolet iS10 FT-IR spectrophotometer (ThermoFisher Scientific Co.) equipped with a deuterated triglycine sulphate (DTGS) detector. The X-ray diffraction (XRD) experiments were performed with a Rigaku D/Max-III-C X-ray (3kW) diffractometer. The sample was exposed to an X-ray beam; the X-ray generator running with a non-monochromated Cu Ka radiation source with a wavelength of 1.54 nm (tube voltage = 40 kV, tube current = 20 mA) and a diffracted beam monochromator at room temperature. The relative intensity was recorded at ambient temperature over an angular range (2θ

degrees) of 5 - 70°. The crystallinity index (*CrI*) was determined using Equation 13 (Ibitoye et al., 2018; Liu et al., 2012):

$$CrI = \left(\frac{I_{110} - I_{am}}{I_{am}} \right) \times 100 \quad (13)$$

where I_{110} is the maximum intensity at $2\theta \approx 19^o$ and I_{am} the intensity of amorphous diffraction at $2\theta \approx 12^o$.

The Scanning Electron Microscopy (SEM) and the Scanning Transmission Electron Microscopy (STEM) analyses were carried out with a Jeol JSM-7600F Field Emission Scanning Electron Microscope operating at an accelerating voltage of 15 kV, equipped with a JED-2300T energy dispersive X-ray spectroscopy (EDS) analysis detector unit to study the morphology and composition of the samples respectively. The nitrogen adsorption and desorption experiments (ASAP2010 Micrometric Inc. USA) were further used to confirm the Brunauer-Emmett-Teller (BET) surface area of the samples.

RESULTS AND DISCUSSION

The chitin yield obtained from crab and shrimp shell wastes ranged from 2.45-4.88 g (i.e. 9.80-19.52%) and 3.20-6.42 g (that is, 12.80 - 25.48%) respectively. This is indicative that maximum yield was obtained from shrimp shell wastes. The extracted chitosan from 45 g of dried waste of Lagoon crab (*C. amnicola*) and pink shrimp (*P. notialis*) was in the range of 2.64 - 5.77 g (5.87 - 12.82%) and 4.27 - 7.52 g (9.49 - 16.71%) respectively. In our studies (Amoo et al., 2019; Olafadehan et al., 2020), exhaustive investigations were carried out to determine the optimum conditions for the yield of the derived chitin and the derived chitosan from crab and pink shell wastes, as well as the degree of deacetylation of chitosan obtained from these precursors. The optimization studies through BBD using response surface methodology gave rise to the respective optimum conditions for the maximum yields of derived chitin and derived chitosan polymers and the maximum derived chitosan DDA from pink shrimp shell wastes as (3.25 mol/dm^3 hydrochloric acid aqueous solution, a demineralization time of 19.03 h, 2.43 mol/dm^3 of sodium hydroxide aqueous solution and a deproteinization time of 2.03 h), (a concentration of 50% w/w NaOH aqueous solution, a deacetylation temperature of 87.9°C and a deacetylation period of 145.26 min) and (NaOH solution of 50% w/w concentration, temperature for deacetylation=97.2°C and a deacetylation time of 90 min) (Amoo et al., 2019). Equally, the optimized chitin extraction conditions from crab shell wastes based on the yield (4.84 g or 19.36%) were reported in our studies (Olafadehan et al., 2020) as 3.25 mol/dm^3 HCl aqueous solution, period of demineralization of 18.55 h, 2.39 M NaOH aqueous solution and period of deproteinization of 2 h while the maximum chitosan yield (5.98 g or 13.29%) was obtained at modeled optimized conditions of 50% w/w NaOH aqueous solution, deacetylation temperature and time of 85.05°C and 133.64 min respectively. The modeled optimization conditions for the extraction process of the derived polymer that modeled the highest *DDA* of chitosan produced from crab shell waste were reported in our studies (Olafadehan et al., 2020) to be 50% w/w NaOH aqueous solution and temperature and time of deacetylation of 84.46°C and 187 min respectively, with the corresponding predicted *DDA* of 84.20%. These were the conditions used to produce the chitin and chitosan whose properties were exhaustively investigated and presented in this study.

Characterization of the extracted chitin and chitosan

The physicochemical properties, proximate analysis, functional groups, crystallinity, elemental compositional percentages and surface morphology of the precursors and their respective extracted chitin and chitosan are presented. These samples were characterized with BET surface area, FTIR, XRD, EDS, SEM and STEM.

Physicochemical properties

The physicochemical properties of shrimp and crab shell wastes (used as the precursors for the extraction of chitin and chitosan) and the chitosan produced from both shrimp and crab shell wastes are presented in Table 1.

Surface area analysis

The results of BET surface area of the precursors and the extracted chitin and chitosan are presented in Table 1. It is thus observed that the specific surface areas (S_{BET}) of the precursors (shrimp and crab shell wastes) are relatively low in comparison to the extracted chitin and chitosan. The specific surface areas of the optimized chitin, raw chitosan and refined (decolorized) chitosan extracted from shrimp shell wastes were calculated to be 5.65, 7.76 and 8.91 m^2/g respectively. Also, the specific surface areas of the optimized chitin, raw chitosan and refined (decolorized) chitosan extracted from crab shell wastes were obtained as 5.50, 7.77 and 8.36 m^2/g respectively. On comparison of the surface areas of the extracted chitin and chitosan in Table 1, it can be inferred that the extracted refined chitosan from shrimp and crab shell wastes had relatively the highest surface area amongst all the prepared materials. This indicates that the refined chitosan extracted from shrimp and crab shell wastes possesses the largest pore surfaces, which were developed within their respective matrices. This projects these chitosans as good candidates to be used as developed within their respective matrices. This projects these chitosans as good candidates to be used as

Table 1. Physicochemical properties of *Penaeus notialis* and *Callinectes amnicola* shell wastes, chitin and chitosan produced from them.

Parameter	Precursor		Shrimp shell wastes			Crab shell wastes		
	SSW	CSW	OC	RC	RFC	OC	RC	RFC
S_{BET} (m^2g^{-1})	0.19	0.18	5.65	7.76	8.91	5.50	7.77	8.36
ρ_B (g mL^{-1})	-	-	0.22	0.30	0.32	0.20	0.25	0.30
pH	5.2	5.5	7.1	7.8	8.0	6.8	7.5	7.4
I (mg g^{-1})	-	-	135	142	150	125	138	145
Proximate analysis								
MC (%)	25.5	20.2	7.80	5.16	5.35	5.95	5.00	5.55
AC (%)	19.5	23.8	3.5	1.85	2.00	3.25	2.15	3.10
Protein (%)	42.5	45.7	4.05	3.80	3.65	2.90	3.92	3.85
Fiber (%)	-	-	6.95	8.01	8.85	6.10	8.45	9.04
Lipid (%)	5.32	4.95	1.50	2.00	2.60	1.95	2.30	2.50
Carbohydrate (%)	-	-	76.20	79.18	77.55	79.85	78.18	75.96

SSW, CSW, OC, RC and RFC designate *Penaeus notialis* (pink shrimp) shell wastes, *Callinectes amnicola* (crab) shell wastes, optimized chitin, raw chitosan and refined chitosan respectively. The major difference between RC and RFC is the presence of pigment on the extracted RC and the absence of pigment on the extracted RFC. The effect of the removal of this pigment was studied via the physicochemical characterizations and analytical procedures.

adsorbent for practical or industrial adsorption processes.

Bulk density analysis

The bulk densities of the optimized chitin, raw chitosan and refined chitosan from shrimp and crab shell wastes obtained in this study are presented in Table 1. These results revealed that the refined chitosan had higher bulk densities than the optimized chitin and raw chitosan. Hence, the use of this material in an adsorption process will ultimately lead to an efficient adsorption process since when added to water, it will sink thereby enhances intimate contact with the adsorbate. Moreover, a higher bulk density signifies greater volume activity. Thus, the refined chitosan from shrimp and crab shell wastes will be a high-quality adsorbent.

pH analysis

Table 1 shows the pH of shrimp and crab shell wastes, the optimized extracted chitin, raw chitosan and refined chitosan. It can be seen that pH of the precursors in water suspension is acidic, which indicates that the use of these precursors as adsorbent may result in a reduced absorption of the adsorbate ions. This is attributable to the fact that there will be increased competitiveness amongst the hydrogen ions and the adsorbate molecules for the same adsorption sites. The pH values obtained for the optimized extracted chitin, raw chitosan and refined chitosan from shrimp and crab shell wastes were in consonance with the observations, findings and inferences drawn by Walther (1983). These values were in the alkaline region, most especially for the refined chitosan from shrimp shell waste. This buttresses the fact that this refined chitosan is regarded as the best adsorbent for industrial applications since increased alkalinity enhances the rate of adsorption of the adsorbate owing to the predominant presence of hydrated species of the adsorbates, changes in the electric charge of surface molecules and the precipitation of the appropriate salt.

Iodine number analysis

The iodine test is a test method that determines the amount of iodine adsorbed (in milligrams) by 1 g of adsorbent under test conditions (Olafadehan et al., 2012). Table 1 gives the iodine number of the precursors, optimized chitin, raw chitosan and refined chitosan obtained from shrimp and crab shell wastes. The refined chitosan from shrimp and crab shell wastes had the highest iodine values of 150 and 145 mg/g respectively amongst all other prepared materials, thereby signifying that their respective pore surfaces and particle structures were the best developed in this study since a higher iodine number usually signifies a higher degree of porosity and activation.

Proximate analysis

The proximate analysis of a material examines its

chemical composition. It is a means of determining the distribution of products obtained when the sample is heated under specified conditions. In this study, the proximate analysis parameters investigated are moisture content (MC), ash content (AC), protein, fiber, lipid and carbohydrate contents.

The moisture content of a sample refers to the percentage of water that resides within the sample. The moisture content should be taken into account when evaluating the relative capacities of different carbon materials for the adsorption of an adsorbate. Ambarish and Sridha (2015) alluded that the percentage moisture content in a typical/commercial derived chitin from shrimp should be about 21. The moisture content (MC) of the crab and shrimp shells were obtained as 20.2 and 25.5% respectively, as shown in Table 1. This shows that the shrimp shell wastes retained more water than crab shell wastes. The extracted chitin, raw chitosan and refined chitosan from shrimp and crab shell wastes had moisture contents of (7.80, 5.16, and 5.35%) and (5.95, 5.00, and 5.55%) respectively. These results were in agreement with KFDA (1995), which stated that the moisture content of a typical/commercial chitosan biopolymer should not be up to 10%. The differences in the moisture contents of the derived biopolymers could most likely be associated to the agglomeration of the amount of moisture absorbed by the different chitin and chitosan biopolymers after several processes of synthesis. Generally, the results showed a drastic reduction in the moisture contents of the extracted biosorbents in comparison to their precursors. A higher moisture content in a material results in reduced capacity of adsorption as well as the effectiveness of the material as an adsorbent due to dilution (Yousef and El-Eswed, 2009; Abubakar et al., 2012). Hence, the precursors (pink shrimp and crab shell wastes) will not be better adsorbents than the derived polymers from them. It is thus recommended that these shell wastes should not be used as adsorbents.

The ash contents (AC) of the extracted optimized chitin from crab and shrimp shell wastes were obtained to be 3.25 and 3.5% respectively while those of raw chitosan for both crab and shrimp shell wastes were obtained as 2.15 and 1.85% respectively, with the values of 3.10 and 2.00% for the refined chitosan from the crab and shrimp shell wastes respectively. The ash content of a sample is the inorganic residue left after the organic matter has been burnt off. Also, the ash content depends on the carbon source and it can serve as a disturbance and interference during the adsorption process (Akyeampong, 1999; Khan et al., 2009). This indicates that a starting material with a resulting high ash content cannot give rise to a promising derived adsorbent so a low ash content-starting material is better suited to produce adsorbent. The results in Table 1 showed that the extracted chitosan from shrimp shells proved to be the best material under this category even though the chitosan extracted from crab shells are equally of high quality.

The protein contents of the optimized chitin, extracted raw chitosan, and refined chitosan from shrimp shell wastes were obtained as 4.05, 3.80, and 3.65% respectively while those of the biosorbents extracted from crab shell wastes were obtained as 2.90, 3.92, and 3.85% respectively. The high protein content of the optimized chitin from shrimp shell wastes in relation to that from the crab shell wastes was an indication that it has more nitrogenous substances than that from the latter. This may be due to the effective removal of protein from the crab during the deproteinization process. However, the raw and refined chitosan from shrimp shell wastes had lower protein contents to those of the extracted chitosan from crab waste shells.

The fiber contents of the extracted biosorbents are shown in Table 1. The fiber contents of the extracted optimized chitin, raw chitosan and refined chitosan from shrimp shell wastes were obtained as 6.95, 8.01 and 8.85% respectively while those from crab shell wastes were obtained as 6.10, 8.45 and 9.04% respectively. It can be seen as a common feature for both precursors that there was a gradual increase of fiber contents from optimized chitin to refined chitosan through raw chitosan. The analyses also indicated that the chitins (raw and refined) from crab shell wastes had higher values of fiber content than the ones from shrimp shell wastes. This could be attributed to higher cellulose matter in crab shell wastes than in shrimp shell wastes. Equally, it was found that the fiber contents of the chitosan were higher than that of the chitins from both sources. This is attributable to the elimination of more organic matter from the chitins to obtain the chitosan, which impacted to a great degree on the presence of more fiber in the chitosan biopolymer. Moreover, the fiber content gives a relatively good account on how crystalline the extracted polymers are. The higher the fiber content, it is most likely the higher the crystallinity of the polymers, which will ultimately give rise to a better biosorbent. Hence, chitosan is presumably a better biosorbent than chitin, judging from this result.

The lipid contents of the extracted chitin, raw chitosan and refined chitosan from crab shell wastes were obtained as 1.95, 2.30 and 2.50% respectively while those from shrimp shell wastes were obtained as 1.50, 2.00, and 2.60% respectively as presented in Table 1. These results were not inconsistent with the value reported by Isa et al. (2012) for different sources of extracted chitin.

Table 1 shows the carbohydrate contents of the extracted chitin, raw chitosan and refined chitosan from shrimp and crab shell wastes, which were (76.20, 79.18, and 77.55%) and (79.85, 78.18, and 75.96%) respectively. The carbohydrate content of the extracted chitin from crab shell wastes was higher than that from the shrimp shell wastes while the carbohydrate contents of the extracted chitosan (raw and refined) from shrimp shell wastes were higher than those from the crab shell waste since the deacetylation process had more effect on

Table 2. FTIR bands of chitin isolated from shrimp and crab waste shells.

Functional group and vibrating modes	Classification	Shrimp chitin wavelength (cm^{-1})	Crab chitin wavelength (cm^{-1})
O—H stretching	—	3470-4040	3471-4047
N—H stretching	—	3112-3268	3113-3260
CH_3 symmetrical stretch and CH_2asymmetric stretch	Aliphatic compounds	2927	2929
CH_3 symmetrical stretch	Aliphatic compound	2864	2870
C═O secondary amide stretch	Amide I	1629	1628
C═O secondary amide stretch	Amide I	1617	1619
N—H bend, C—N stretch	Amide II	1558	1553
CH_2 ending and CH_3 deformation	—	1430	1425
CH bend, CH_3 sym. Deformation	—	1382	1383
CH_2 wagging	Amide III, components of protein	1317	1316
Asymmetric bridge oxygen stretching	—	1171-1259	1173-1258
Asymmetric in-phase ring stretching mode	—	1114	1111
C—O—C asymmetric. stretch in phase ring	Saccharide rings	1076	1079
C—O asymmetric stretch in phase ring	—	1026	1026
CH_3 wagging	Along chain	970	968
CH ring stretching	Saccharide rings	900	903

the former precursor than on the latter.

Fourier Transform Infrared Spectroscopy (FTIR)

The Fourier Transform Infrared (FTIR) investigations showed the characteristic wavelengths and spectra of the extracted chitin, raw chitosan and refined chitosan from shrimp and crab shell wastes as presented in Tables 2 to 4 respectively and depicted in Figures 1 and 2 respectively.

Studies in the past have affirmed that there exists α, β and γ polymorphic forms of any extracted chitin (Daraghmeh et al., 2011). The α-crystalline form of the chitin polymer exhibits peaks near 1650, 1620 and 1550 cm^{-1}, which correspond to the following functional groups: C═O secondary amide stretching (Amide I), N—H bending and C—N stretching (Amide II), respectively (Jang et al., 2014). Table 2 and Figures 1(a) and (b) display the FTIR bands for the optimized chitin extracted from the shrimp and crab shell wastes, and those of the precursors. In this study, these bands were observed at 3470-4040, 3112-3267, 1629, 1558, 1317 cm^{-1} and 3471-4047, 3113-3260, 1628, 1553, 1316 cm^{-1} in the FT-IR spectra of the extracted chitin from shrimp and crab shell wastes respectively, as presented in Figures 1(a) and (b), and are attributable to the following modes of the functional groups: O-H stretching, N-H stretching and amides I, II and III, respectively confirming that the optimized chitins from the precursors were in α-crystalline form as revealed in the works of Daraghmeh et al. (2011) and Jang et al. (2014). Equally for shrimp and crab chitin, some other strong and broad bands were respectively observed at 2864 and 2870 cm^{-1} (aliphatic compounds), 1430 and 1425 cm^{-1} (CH_2 ending and CH_3 deformation), 1382 and 1383 cm^{-1} (CH bend, CH_3 symmetrical deformation), 1317 and 1316 cm^{-1} (CH_2 wagging), 1171-1259 and 1173-1258 cm^{-1} (asymmetric bridge oxygen stretching), 1114 and 1111 cm^{-1} (asymmetric in-phase ring stretching mode), 1076 and 1079 cm^{-1} (saccharide rings), 1026 and 1026 cm^{-1} (C-O asymmetrical stretching in-phase ring), 970 and 968 cm^{-1} (along chain), and 900 and 903 cm^{-1} (CH ring stretching, saccharide rings). The values, data and peaks obtained herein were corroborated by those in the works of Ifuku et al. (2009) and Kaya et al. (2014, 2015). The effectiveness and efficiency of the deproteinization process, as decribed in this research, were affirmed by the absence of the 1540 cm^{-1} absorption peak band in the extracted chitin from both the pink shrimp and crab shell wastes. This band mainly confirms and is associated with the protein functional group. However, the absence of this absoprtion band confirms the efficacy of the deproteinization process performed (Majitán et al., 2007).

Tables 3 and 4 show the FTIR bands for the refined (decolorized) and raw (non-decolorized) chitosan extracted from the shrimp and crab shell wastes, as well as the comparison of the experimental FTIR bands of the refined chitosan with the standard from Sigma Aldrich in Germany. In both cases, the % error was $< \pm 5$, confirming the production of chitosan in this study. Figure 2(a) and (b) display the FT-IR bands for the refined and raw chitosan extracted from the shrimp and crab shell waste shell. The spectra of refined chitosan from shrimp shell wastes and those of the crab shell wastes were similar to those of raw chitosan extracted from shrimp

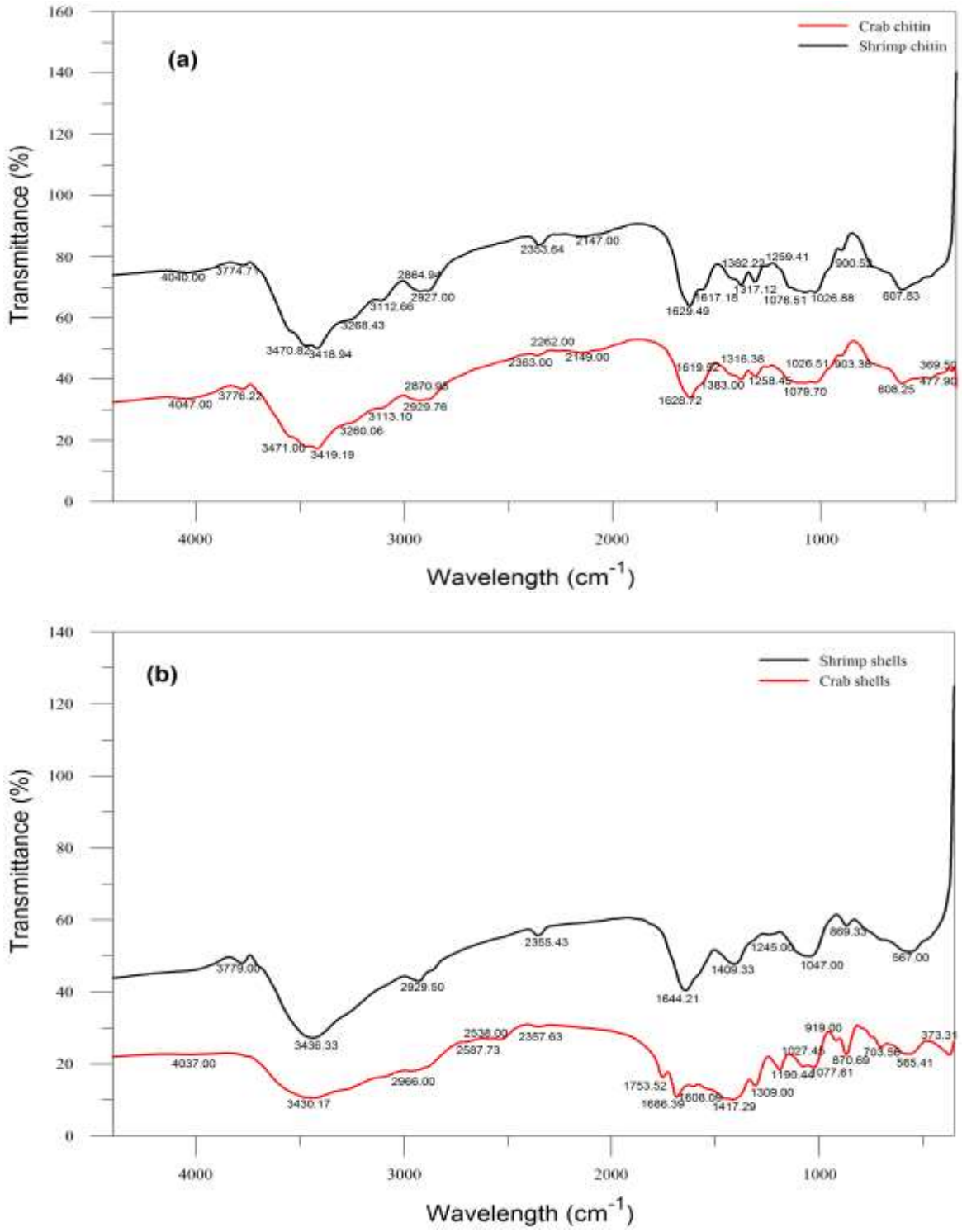

Figure 1. FTIR spectrum of (a) optimized chitin from pink shrimp and crab shell wastes (b) pink shrimp and crab waste shells precursors.

and crab shell wastes, having just some few differences and modifications along their FTIR bands. The refined chitosan from the shrimp and crab shell wastes exhibited broad bands at 3458, 2927, 2359-2891, 1643, 1550 cm^{-1} and 3418-3780, 2928-3204, 2145-2353, 1622, 1515 cm^{-1} respectively (Figure 2a), corresponding to the stretching

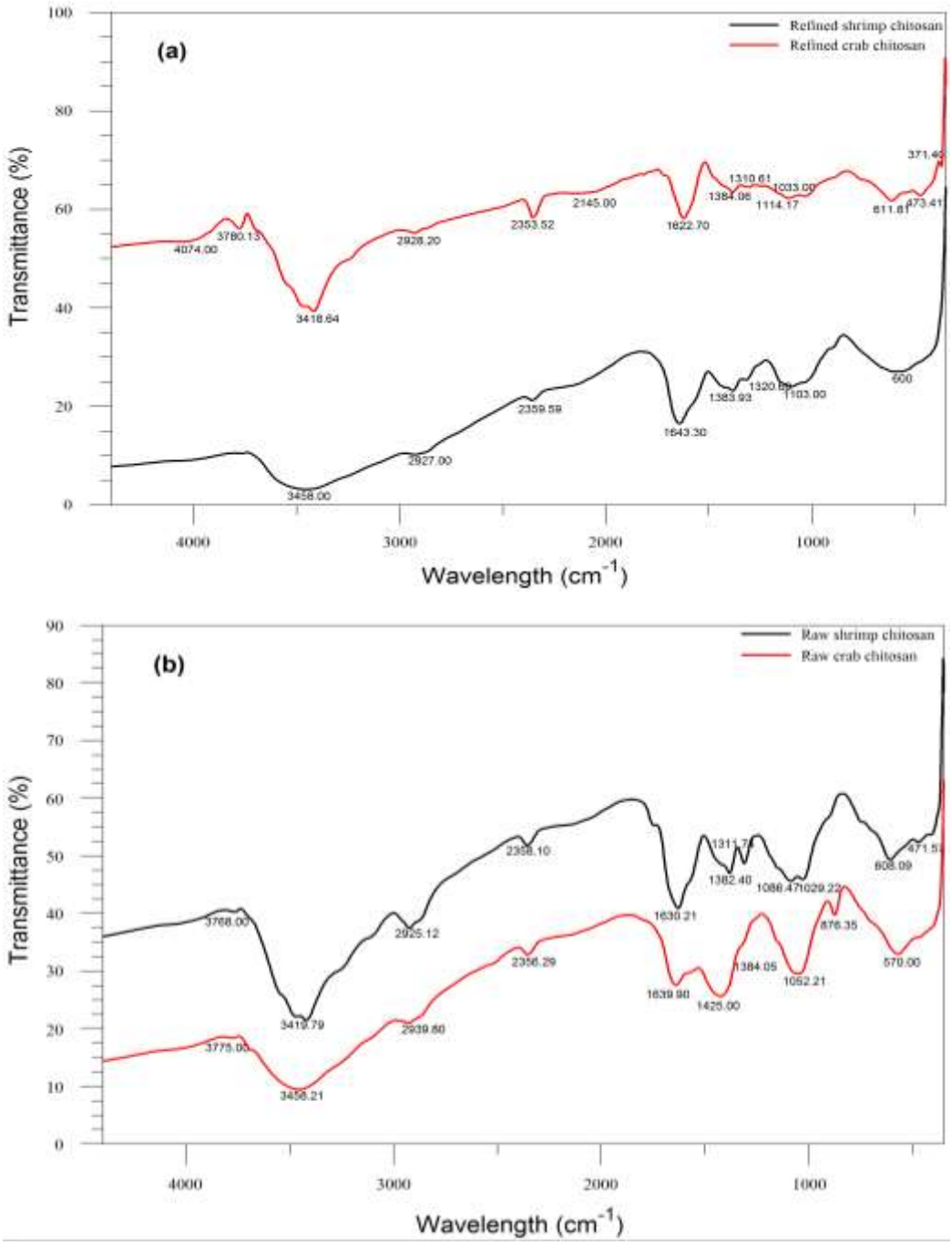

Figure 2. FTIR spectrum of (a) refined chitosan and (b) raw chitosan from pink shrimp and crab waste shells.

vibration of N-H and O-H with intermolecular H_2 bonds of saccharide (poly) and extending vibration of N-H functional group, an asymmetric C-H stretching vibration, symmetric C-H stretching vibration, symmetric C=O stretching vibration, and symmetric N-H stretching vibration. The split of the amide I was predictably missing as observed in refined chitosan from both the shrimp and crab shell wastes (Figure 2a). A characteristic peak at 1550 cm^{-1} and 1515 cm^{-1} shows the success of N-deacetylation process in both pink shrimp and crab types of refined chitosan. The absorption at 1428, 1383, and 1384 cm^{-1} for shrimp and crab shell wastes were due to the C-N stretching vibrations. The band at 1320 cm^{-1} (refined shrimp chitosan) and 1310 cm^{-1} (refined crab chitosan) were attributed to the O-H bending vibration in the pyranose ring (Crews et al., 2009). The complex

Table 3. Comparison of the experimental FTIR bands of chitosan isolated from shrimp shell waste and the standard from Sigma Aldrich.

Parameters / Functional group and vibrating modes	λ_{RFC} (cm^{-1})	λ_{RC} (cm^{-1})	λ_{std} (cm^{-1})	% error, ε
υ (NH_2) associated with primary amines and υ (OH)associated with pyranose ring	3458	3419-3768	3428	±0.88
$\upsilon_{as}(CH_2)$ in CH_2OH group	2927	2925	2923	±0.14
υ (C–H) in pyranose ring	2359-2891	2358	2880	±0.38
υ (C=O) in $NHCOCH_3$ group (amide I band)	1643	1630-1785	1667-1623	±1.44
υ (NH_2) in $NHCOCH_3$ group (amide II band)	1550	1548	Not detected	-
$\delta(CH_2)$ in CH_2OH group	1428	1441	1422	±0.42
$\delta_s(CH_3)$ in $NHCOCH_3$ group	1383	1382	1380	±0.22
δ (C–H) in pyranose ring	1320	1311	1322	±0.15
Complex vibrations of NHCOgroup (amide III band)	1260	Not detected	1262	±0.16
υ_s(C–O–C) (glycosidic linkage)	1143	Not detected	1155	±1.04
υ_{as}(C–O–C) (glycosidic linkage)	1073	1086	1077	±0.37
υ (C–O) in secondary OH group	1069	1029	1074	±0.47
υ (C–O) in primary OH group	1030	742-951	1031	±0.10
Pyranose ring skeletal vibrations	885	888	897	±1.34
δ (NH) out of plane	660	Not detected	664	±0.60
δ (OH) out of plane	614	Not detected	616	±0.32

Table 4. Comparison of the experimental FTIR bands of chitosan isolated from crab shell wastes and the standard from Sigma Aldrich.

Parameters / Functional group and vibrating modes	λ_{RFC} (cm^{-1})	λ_{RC} (cm^{-1})	λ_{std} (cm^{-1})	% error, ε
υ (NH_2) associated with primary amines and υ (OH)associated with pyranose ring	3418-3780	3458-3775	3422	±0.12
$\upsilon_{as}(CH_2)$ in CH_2OH group	2928-3204	2929	2923	±0.17
υ (C–H) in pyranose ring	2865	2356-2890	2879	±0.49
υ (C=O) in $NHCOCH_3$ group (amide I band)	1622	1639	1655-1627	±0.31
υ (NH_2) in $NHCOCH_3$ group (amide II band)	1515	Not detected	Not detected	–
$\delta(CH_2)$ in CH_2OHgroup	1422	1457	1422	0
$\delta_s(CH_3)$ in $NHCOCH_3$ group	1384	1425	1382	±0.14
δ (C–H) in pyranose ring	1310	1384	1322	±0.91
Complex vibrations of NHCOgroup (amide III band)	1255	1247	1257	±0.16
υ_s(C–O–C) (glycosidic linkage)	1114	1120	1077	±3.44
υ_{as}(C–O–C) (glycosidic linkage)	1090	1052	1073	±1.58
υ (C–O) in secondary OH group	1033	1010	1030	±0.29
υ (C–O) in primary OH group	1025	945	1029	±0.39
Pyranose ring skeletal vibrations	890	876	897	±0.78
δ (NH) out of plane	660	654	662	±0.30
δ (OH) out of plane	601	Not detected	605	±0.66

vibrations of NHCO functional group indicating the amide III band were seen at wave numbers 1260 and 1255 cm^{-1} for the refined chitosan from shrimp and crab shell wastes respectively. The C-O stretching vibration in the secondary alcohol was respectively evaluated for shrimp and crab refined chitosan at wave numbers of 1103 and 1114 cm^{-1}. Notwithstanding, a C-O stretch vibration equally in the alcohol functional group was observed at 1073 cm^{-1} (shrimp refined chitosan) and 1090 cm^{-1} (crab refined chitosan). Moreover, absorption bands at 600-835 and 611-797 cm^{-1} were ascribed to the C-H out-of-plane vibration of the ring of monosaccharides. From the FTIR results, we can suggest that the similarity between the chemical composition and bonding types of refined chitosan in the shrimp and crab shell wastes are very close. The raw chitosan from the shrimp and crab shell

Table 5. Degree of deacetylation (*DDA*) of chitosan isolated from shrimp and crab waste shells; Fourier transform infrared (FTIR) and acid-base titration methods.

Parameter	Wave number (cm^{-1})	*T* (%)	*A* -Log (% *T*)	DDA_{FTIR} (%)	DDA_{TITRA} (%)
Refined chitosan (shrimp), optimized	1320.60	25.39	0.5953	82.25	89.73
	1383.93	23.20	0.6343		
Refined chitosan (crab), optimized	1310.61	64.51	0.1904	81.32	84.50
	1384.06	63.56	0.1968		
Raw chitosan (shrimp), optimized	1311.74	48.73	0.3122	81.79	84.76
	1382.40	47.01	0.3278		
Raw chitosan (crab), optimized	1384.05	27.47	0.5611	81.94	82.15
	1425.00	25.59	0.5919		

A and *T* represent absorbance and transmittance respectively.

wastes also showed broad bands at 3419-3768, 2925, 2358, 1630-1785, 1548 cm^{-1} and 3458-3775, 2929, 2356-2890, 1639 cm^{-1} respectively (Figure 2b), corresponding to the stretching vibration of N-H and O-H with the extension vibration of N-H and the intermolecular hydrogen bonds of polysaccharide, asymmetric C-H stretching vibration, symmetric C-H stretching vibration, symmetric C=O stretching vibration, and symmetric N-H stretching vibration. The absorption band at 1548 and 1120 cm^{-1} also revealed the success of N-deacetylation in both shrimp and crab types of raw chitosan (Figure 2b) with similar prominent characteristic bands. The absorption at (1441, 1382 cm^{-1}) and (1457 and 1425 cm^{-1}) for shrimp and crab shell wastes respectively, were also due to the C-N stretching vibrations. The bands at 1311 cm^{-1} (raw shrimp chitosan) and 1384 cm^{-1} (raw crab chitosan) were equally associated with the O-H bending vibration in the pyranose ring of the extracted biopolymers. The complex vibrations of NHCO group indicating the amide III band were seen at wave number 1247 cm^{-1} for the raw chitosan from crab shell wastes. The C-O stretching vibration in the secondary alcohol was evaluated for crab raw chitosan at a wave number of 1120 cm^{-1}. Nevertheless, a C-O stretching vibration in the alcohol was seen at 1086 cm^{-1} (shrimp raw chitosan) and 1052 cm^{-1} (crab raw chitosan). Also, the absorption bands and peaks at wavelengths of 471-608 and 876 cm^{-1} were ascribed to the C-H out-of-plane vibration of the ring of monosaccharides as shown in Figure 2(b). From the corresponding FTIR results, it can be inferred that the resemblance and equivalence between the chemical compositional structure and bonding types of the refined chitosan and raw chitosan extracted from the shrimp and crab shell wastes are very close with close similarity with the standards obtained from Sigma Aldrich and can, therefore, be substituted for each other during practical usage.

The degree of deacetylation (*DDA*) of the refined chitosan and raw chitosan from the shrimp and crab shell wastes was calculated thus (Ghimire et al., 2011):

$$\%\ DDA = 100 - \frac{1}{0.03133}\left(\frac{A_{1320}}{A_{1420}} - 0.3822\right) \qquad (14)$$

where A_{1320} and A_{1420} are the absorbance at wavelengths 1320 cm^{-1} and 1420cm^{-1} (%) respectively.

The FTIR calculated *DDA*, DDA_{FTIR}, and the *DDA* obtained from the acid-base titration method, DDA_{TITRA}, for the refined and raw chitosan from the shrimp and crab shell wastes are presented in Table 5.

The DDA_{FTIR} and DDA_{TITRA} of the refined chitosan from shrimp shell wastes were obtained as 82.25 and 89.73% respectively; with % error of 8.34 while the DDA_{FTIR} and DDA_{TITRA} values of the refined chitosan from crab waste shells were found to be 81.32 and 84.50% respectively giving % error of 3.76. Similarly, the DDA_{FTIR} values of the raw chitosan from shrimp shell wastes and crab waste shells were calculated as 81.79 and 81.94% respectively while the DDA_{TITRA} of the raw chitosan from shrimp and crab shell wastes were obtained as 84.76 and 82.15%. The percentage errors obtained from the DDA_{FTIR} and DDA_{TITRA} of the extracted chitosan from shrimp and crab shell wastes were 3.50 and 0.26 respectively. The relatively low % error values confirm that the acid-base titration method of obtaining the degree of deacetylation of chitosan is effective, efficient, and reliable while the degree of deacetylation of chitosan determined by using the Fourier transform infrared spectra (DDA_{FTIR}) is substantiated by the values obtained from the acid-base titration methods. It was also observed that the titration method gave DDA_{TITRA} values higher for all the types of extracted chitosan than the FTIR calculated *DDA* (DDA_{FTIR}), which was in agreement with the observation of Ghimire et al.

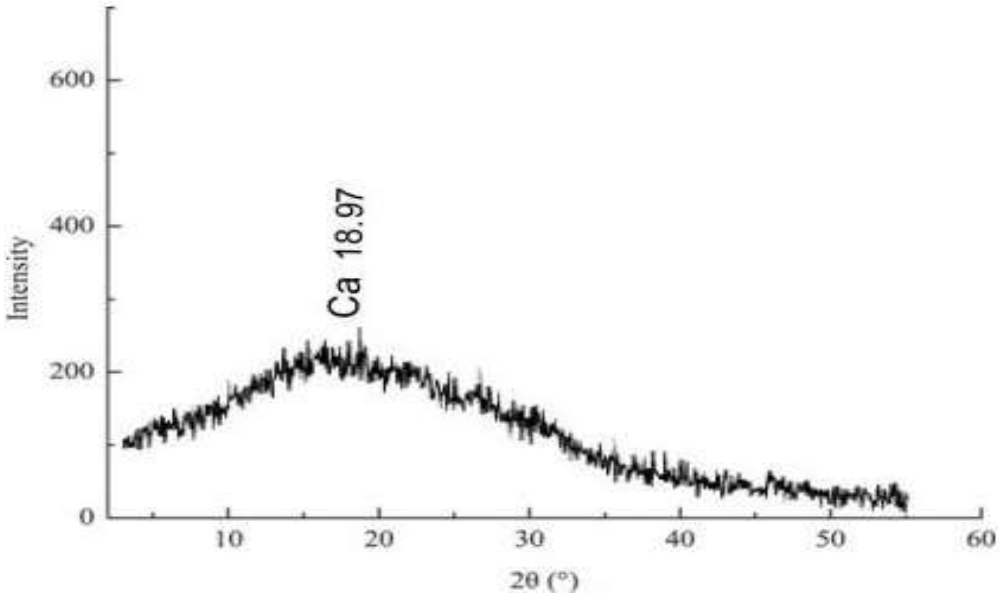

Figure 3. XRD pattern of pink shrimp shell wastes.

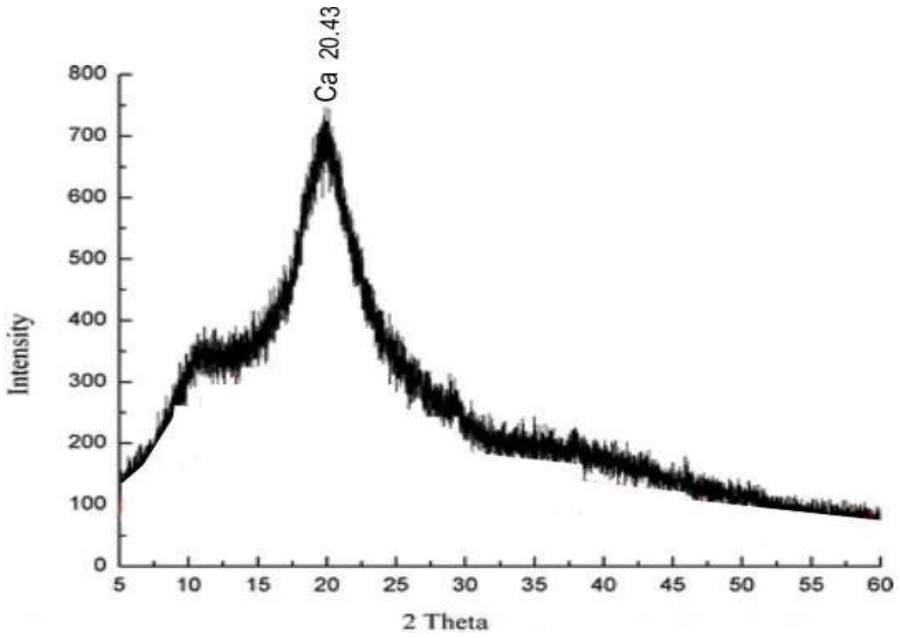

Figure 4. XRD pattern of crab shell wastes.

(2011). However, the values of the *DDA* of chitosan extracted from both FTIR and acid-base methods in Table 5 are within the commercial range of 30-95% (Sarbon et al., 2014).

X-ray diffraction (XRD)

X-ray diffraction (XRD) analysis was performed on the samples to verify, validate and evaluate the degree of crystallinity of the isolated chitin and chitosan. The precursors (that is, shrimp and crab shell wastes) were characterized by powder X-ray diffraction as shown in Figures 3 and 4. The diffractogram results (Figure 3) of shrimp shell wastes scanned between 2θ (deg) = 5 and55° reveal a total of ten peaks at 5.5°, 7.5°, 15.9°, 18.97°, 20.1°, 25.4°, 30.6°, 40.9°, 50.0° and 55.3°, while the diffractogram results of crab shell wastes precursor

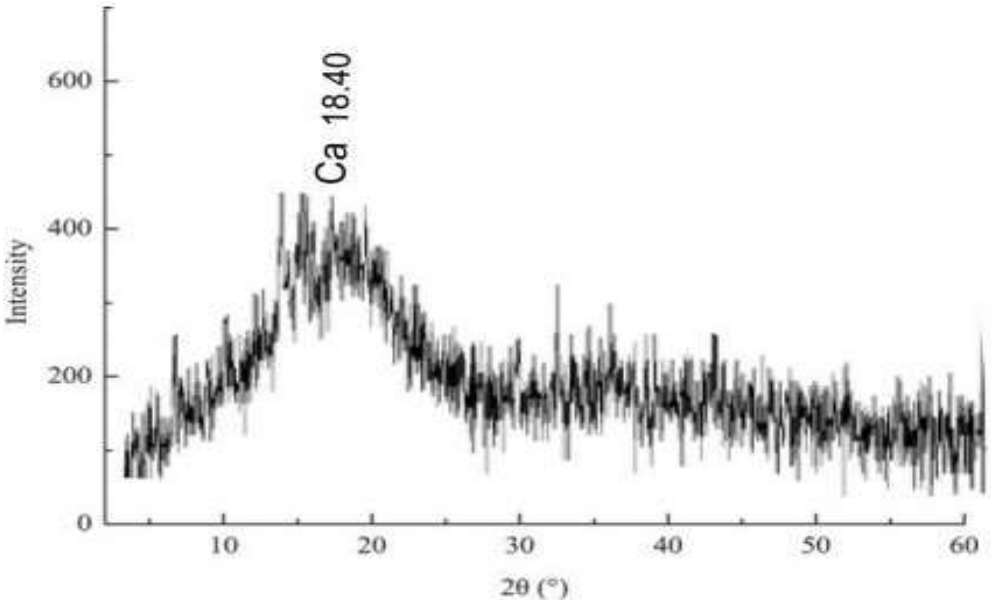

Figure 5. XRD pattern of chitin from pink shrimp shell wastes.

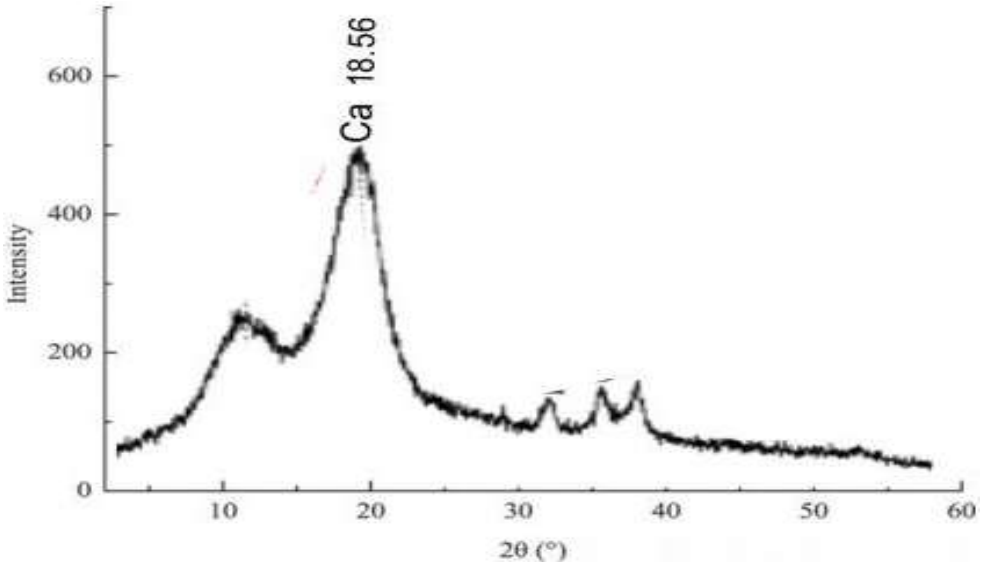

Figure 6. XRD pattern of chitin from crab shell wastes.

scanned between 2θ (deg) = 5 and 60° in Figure 4 shows a total of nine peaks at 5.6°, 10.8°, 15.2°, 20.4°, 25.9°, 30.9°, 40.0°, 50.9° and 54.8°.

The X-ray diffraction patterns for the chitin extracted from shrimp and crab shell wastes are shown in Figures 5 and 6 respectively. The XRD patterns indicate that both the positions and intensities of the Bragg peaks of the extracted chitin show resemblance in patterns to those of other works from different precursors in literature (Liu et al., 2012; Ifuku et al., 2009; Fan et al., 2008); Fan and Saito, 2009). In Figure 5, the diffractogram results of chitin from shrimp shell wastes scanned between 2θ (deg) = 5 and 60° show a total of twelve peaks with three strong peaks at 15.6°, 18.4°, and 38.2° and nine weak ones at 7.1°, 12.5°, 25.2°, 30.2°, 33.21, 40.3°, 45.1°, 50.2° and 60.3° while the X-ray diffraction (XRD) results of the extracted chitin from crab shell wastes as shown in Figure 6 scanned between 2θ (deg) = 5 and 60° show a total of nine peaks with two strong peaks at 15.26° and18.56° and seven weak ones at 5.96°, 10.8°, 25.84°,

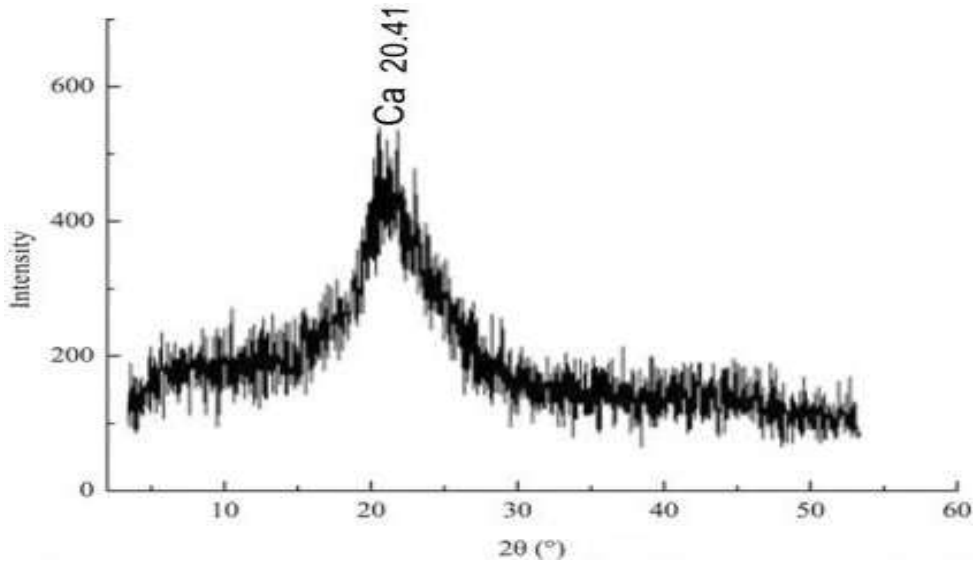

Figure 7. XRD pattern of refined chitosan from pink shrimp shell wastes.

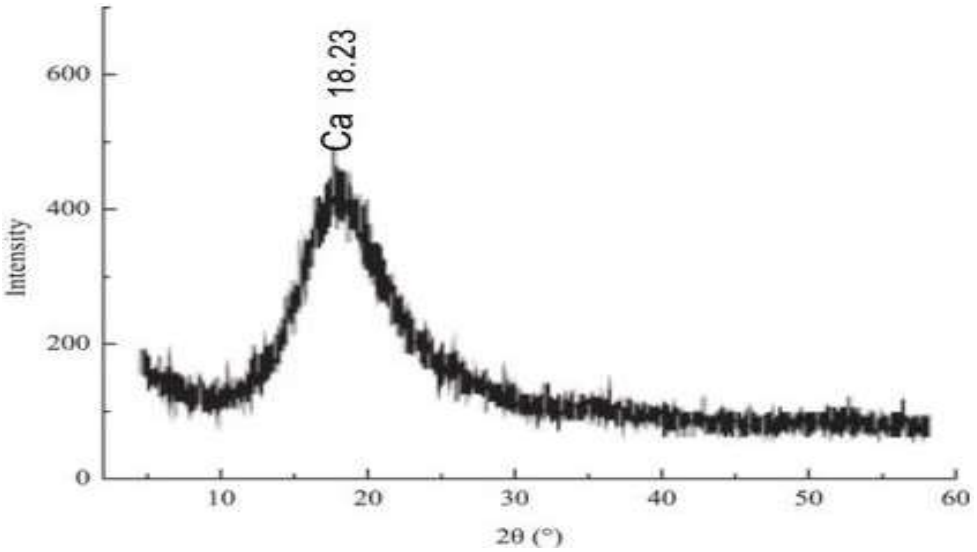

Figure 8. XRD pattern of raw chitosan from pink shrimp shell wastes.

30.9°, 40.0°, 50.86° and 54.8° respectively.

The refined chitosan extracted from shrimp shell wastes was also characterized using X-ray diffraction (XRD). The diffractogram, shown in Figure 7, illustrates the results obtained for the extracted refined chitosan from shrimp shell wastes with 2θ (deg) scanned from 5 to 55° having a total of nine peaks with three strong peaks at 20.4°, 25.2° and 30.4°, and six weak ones at 5.5°, 10.5°, 15.86°, 40.6°, 50.9° and 54.0° while the diffractogram results of the extracted raw chitosan from shrimp shell wastes in Figure 8 scanned between 2θ (deg) = 5 and 60° show a total ten peaks with three strong peaks at 15.4°, 18.2° and 25.0°, and seven weak peaks at 5.3°, 10.5°, 30.5°, 35.1°, 40.0°, 50.5° and 58.5° respectively. The similarity in these Bragg peaks confirms that the extracted refined and raw chitosan were of required specifications.

The diffractogram results of the extracted refined chitosan from crab shell wastes as shown in Figure 9 being scanned between 2θ (deg) = 7 and 75° show a total of ten peaks at 7.38°, 10.65°, 14.46°, 16.67°, 20.43°, 25.64°, 30.22°, 39.45°, 50.4° and 60.43°. The broad Bragg peaks occurred at four different locations along the scanned 2θ (deg) = 7-75° at 14.46°, 20.43°, 25.64° and

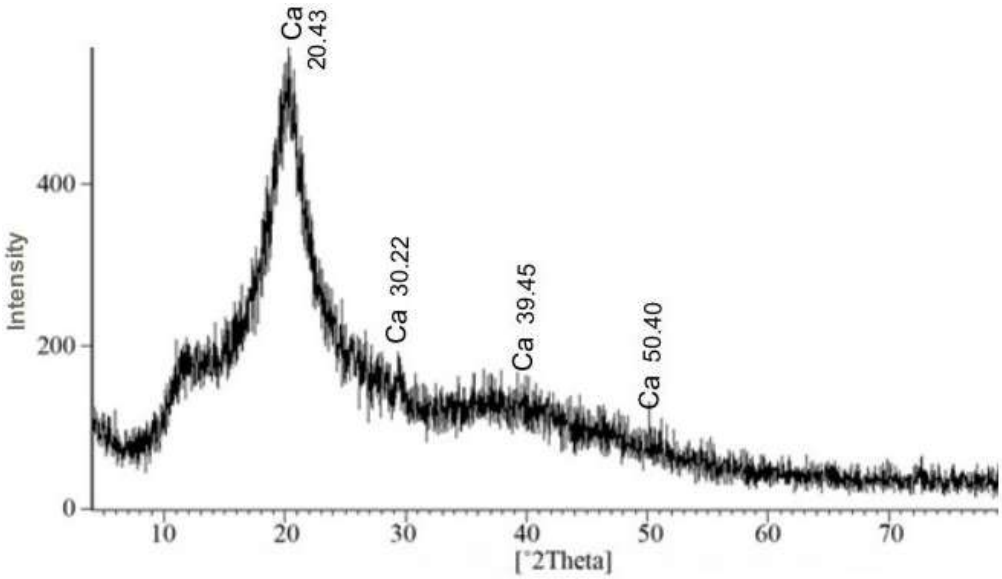

Figure 9. XRD pattern of refined chitosan from crab shell wastes.

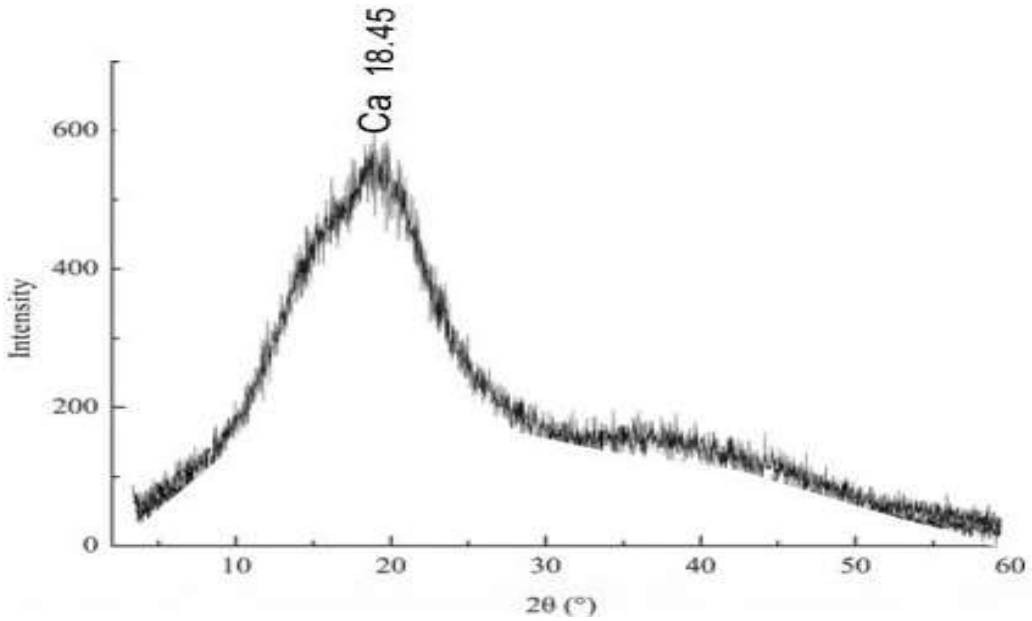

Figure 10. XRD pattern of raw chitosan from crab shell wastes.

39.45° while the rest are weak peaks. Furthermore, raw chitosan extracted from crab shell wastes was also characterized using X-ray diffraction (XRD) giving a diffractogram shown in Figure 10. The results were scanned between 2θ (deg) scanned from 5 to 60° having a total of ten peaks with three strong peaks at 14.66°, 16.27° and 18.45°, and seven weak ones at 7.35°, 10.5°, 25.24°, 30.1°, 40.2°, 50.35° and 60.1° respectively. Thus, the obtained XRD diffractograms for both the refined and raw chitosan show that both the positions and intensities of the Bragg peaks of the extracted chitosan matched patterns described by other works in literature (Liu et al., 2012; Ifuku et al., 2009).

The crystallinity index, *CrI*, values of chitin and its derivatives play a major role in the determination and effectiveness of their applications. In this study, the *CrI* of the extracted chitin obtained from shrimp shell wastes (60.0%) is relatively lower than the value obtained for the

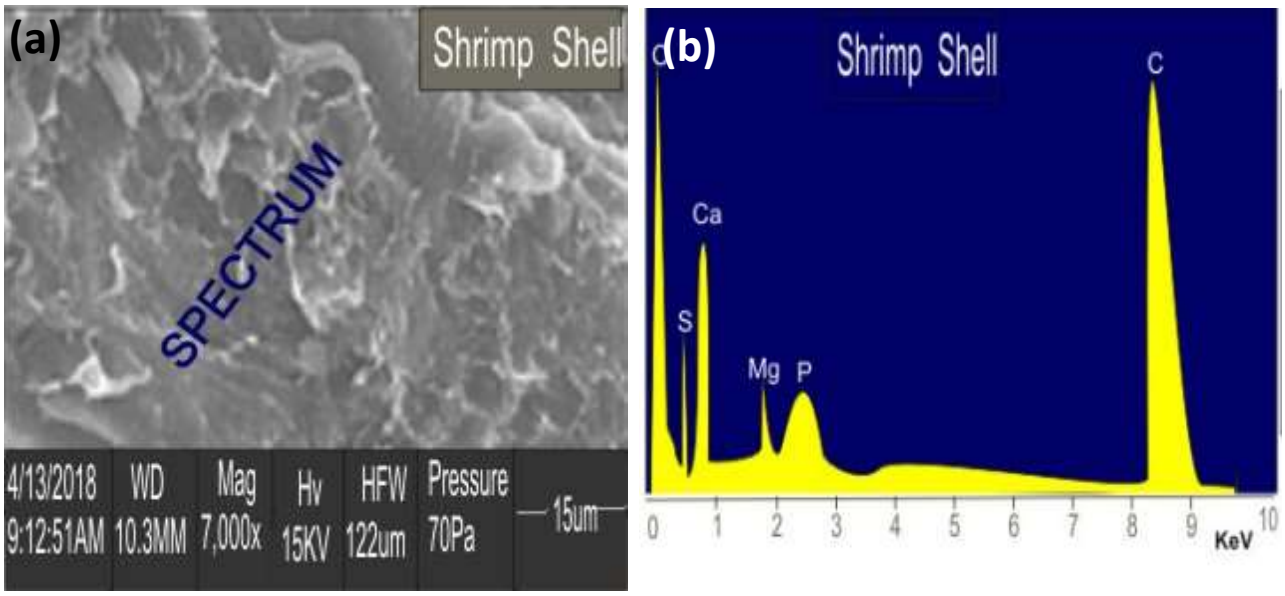

Figure 11. (a) BSED image of the pink shrimp shell precursor showing the spectrum in which EDS analysis was carried out and (b) the corresponding EDS spectrum at the specified spectrum point as indicated in (a).

extracted chitin from crab shell wastes (70.0%), signifying that the latter is more crystalline than the former. Equally, the crystallinity index values the extracted refined chitosan from shrimp and crab shell wastes were obtained as 74.36 and 68.33% respectively while the CrI values of the raw chitosan from shrimp and crab shell wastes were obtained as 64.0 and 60.0% respectively. These results show that the refined chitosan from shrimp shell wastes is more crystalline than any of the other extracted chitosan from the specified sources.

Surface composition

The identification and recognition of the surface properties and composition of the prepared biosorbents are germane in the comprehension of the role and function of the biosorbents on adsorption processes. The presence of elements and the corresponding composition are evaluated using energy dispersive X-ray spectroscopy (EDS). Figure 11(a) shows the Back Scattered Electron Diffraction (BSED) image of the shrimp shell wastes precursor with its corresponding sample spectrum taken. The corresponding EDS spectrum is shown in Figure 11(b), which also indicates that the shrimp shell wastes used as a precursor for the biosorbents contain C and O_2. Ca, O_2, and C showed the highest peaks in the EDS spectrum while elements such as S, P and Mg showed relatively low peaks signifying their minute amounts present in the composition of the shrimp shell wastes. The EDS compositional analysis obtained on the spectrum of the shrimp shell wastes shows the presence of O_2, sulphur, carbon, calcium with a weight percent of 44.4, 10.0, 28.0 and 18.2 respectively. Other trace elements such as phosphorus and magnesium on the spectrum had weight percentages of 3.4 and 4.8 respectively.

The compositional analysis of the crab shell wastes precursor is shown in the Back Scattered Electron Diffraction (BSED) image in Figure 12(a). The analysis was carried out on the area stated as a spectrum across the sample, as shown in Figure 12(a). The analogous EDS spectrum is corroborated by Figure 12(b), wherein it was seen that the crab shell wastes used as a precursor for the adsorbents contained carbon, sulphur and oxygen. Furthermore, calcium, oxygen and calcium showed the highest peaks in the EDS spectrum while the other elements such as sulphur, phosphorus and magnesium showed relatively low peaks, signifying their minute amounts present in the composition of the crab shell wastes. The EDS compositional analysis of the crab shell wastes as obtained from the spectrum shows the presence of the elements present in the material: S, O_2, C, Ca, P and Mg with weight percents of 8.4, 30.1, 23.0, 25.5, 10.4 and 2.8 respectively.

Figures 13(a) and (b) show the respective BSED image of the extracted chitin from shrimp shell wastes with the compositional testing point (spectrum) and the corresponding Energy Dispersive X-ray spectroscopy (EDS) pattern of testing point, spectrum. The corresponding EDS spectrum of BSED image of the extracted chitin from shrimp shell wastes is shown in Figure 13(b), wherein it was indicated that the produced chitin from shrimp shell wastes contained carbon, calcium and oxygen. Carbon and oxygen showed the highest peaks in the EDS spectrum while the other elements

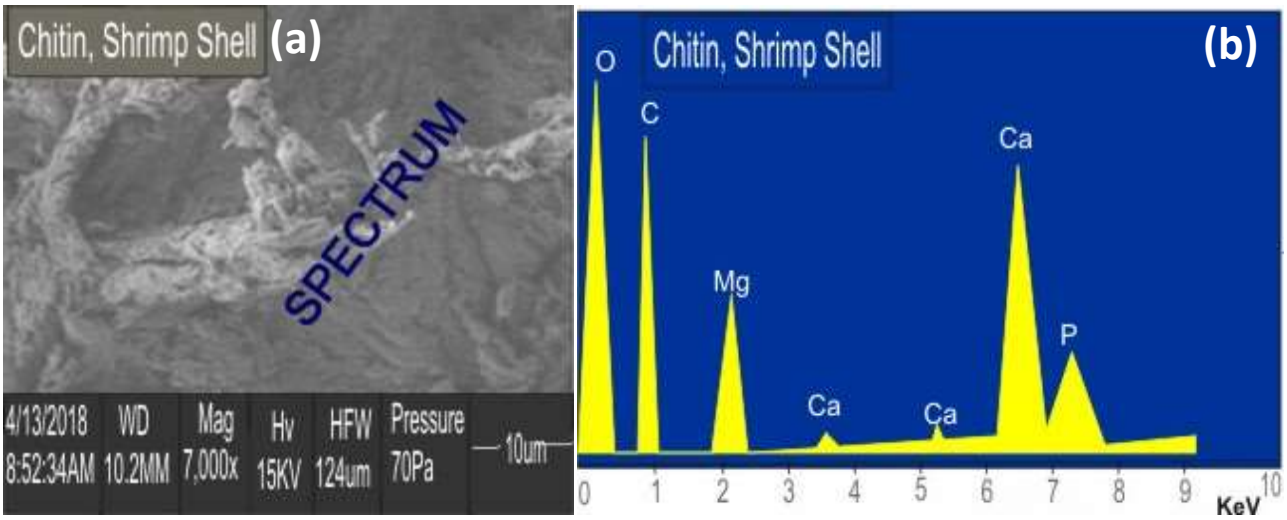

Figure 13. (a) BSED image of the chitin from pink shrimp shell precursor showing the spectrum in which EDS analysis was carried out and (b) the corresponding EDS spectrum at the specified spectrum point as indicated in (a).

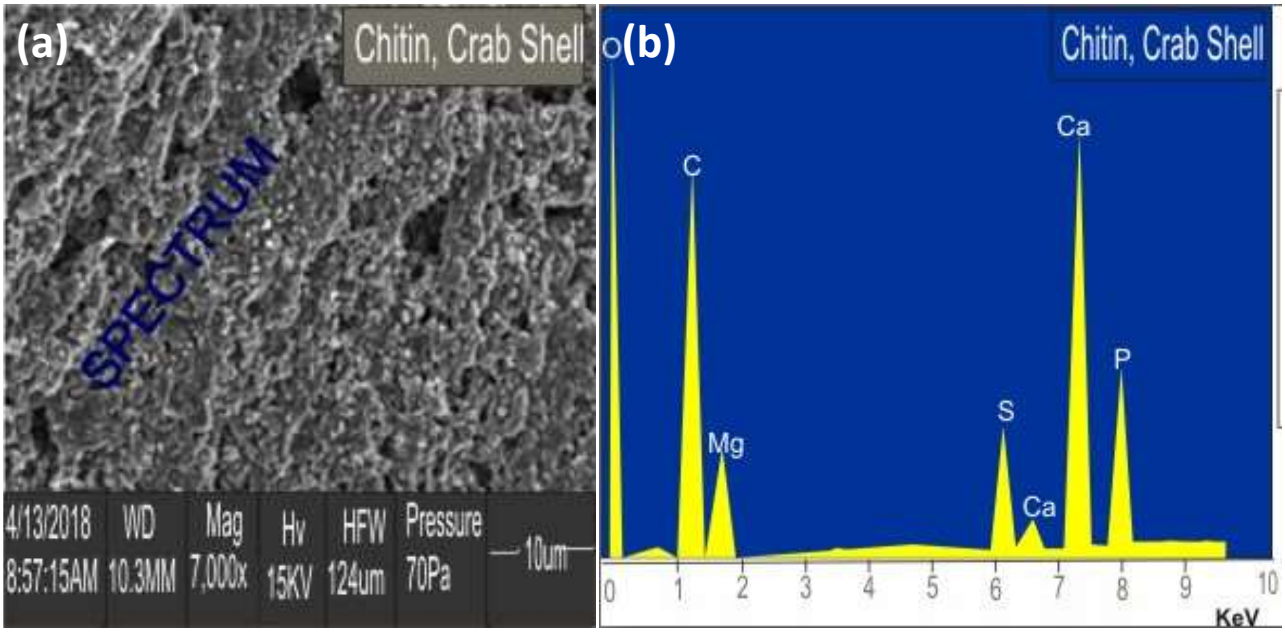

Figure 14. (a) BSED image of the chitin from crab shell precursor showing the spectrum in which EDS analysis was carried out and (b) the corresponding EDS spectrum at the specified spectrum point as indicated in (a).

such as phosphorus, calcium and magnesium showed relatively low peaks, signifying their minute amounts present in the composition of the extracted chitin from shrimp shell wastes. It was observed that the elemental sulphur that was present in the precursors (shrimp and crab shell wastes) is absent in the extracted chitin from shrimp shell wastes. The EDS compositional analysis obtained on the spectrum of the extracted chitin from shrimp shell wastes confirmed the presence of oxygen with a weight percent of 35.0, carbon (40.0 wt%), phosphorus (1.5 wt%), magnesium (7.7 wt%) and calcium (1.5 wt%).

Figure 14 shows the respective BSED image of the extracted chitin from crab shell wastes with the compositional testing point (spectrum) and the corresponding Energy Dispersive X-ray spectroscopy (EDS) pattern of testing point, spectrum. The corresponding EDS spectrum of BSED image of the

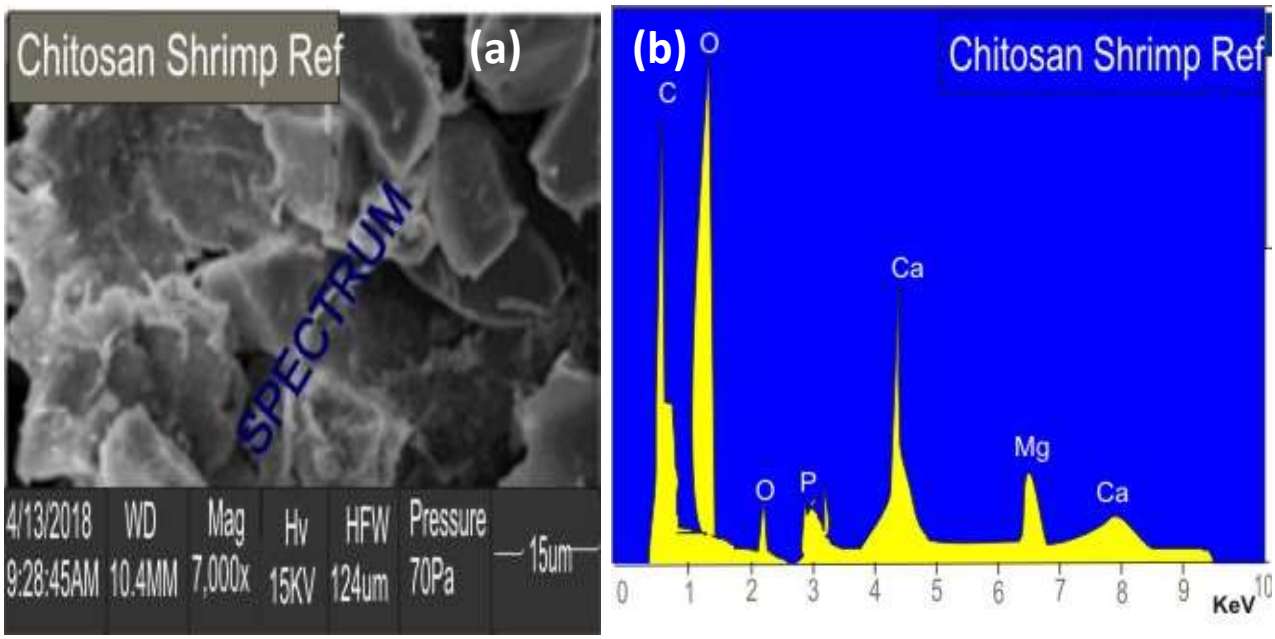

Figure 15. (a) BSED image of the refined chitosan from pink shrimp shell precursor showing the spectrum in which EDS analysis was carried out and (b) the corresponding EDS spectrum at the specified spectrum point as indicated in (a).

extracted chitin from crab shell wastes is shown in Figure 14(b), which signifies that the produced chitin biosorbent from crab shell wastes contains carbon, calcium and oxygen. Additionally, carbon, oxygen and calcium exhibited the highest peaks in the EDS spectrum while the other elements such as phosphorus, sulphur and magnesium showed relatively low peaks when compared with those of Ca, C and O_2 thereby signifying their minute amount present in the composition of the extracted chitin from crab shell wastes. It was observed that the elemental sulphur that was present in the precursors (shrimp and crab shell wastes) is just about present in a greatly reduced amount in the extracted chitin from crab shell wastes. The EDS compositional analysis obtained on spectrum of the extracted chitin from shrimp shell wastes confirmed the presence of oxygen, carbon, phosphorus, magnesium and calcium with weight percentages of 40.0, 20.0, 6.4, 3.8 and 26.0 respectively.

The BSED image of the refined chitosan from shrimp shell wastes is shown in Figure 15(a), with specific testing points (spectrum) for the Energy Dispersive X-ray Spectroscopy (EDS) analysis to be carried out. Figure 15(b) shows the corresponding EDS composition analysis plot for the testing point of the specific spectrum. The EDS plot shows carbon peaks at 0.56 keV, oxygen peaks at 1.5 keV and 2.1 keV, phosphorus peaks at 3.02 keV, calcium peaks at 4.5 keV and 7.9 keV, and magnesium peaks at 6.5 keV. Figure 15(b) shows that the extracted chitosan biosorbent from shrimp shell wastes also contain carbon, calcium and oxygen. Additionally, carbon and oxygen exhibited the highest peaks in the EDS spectrum while the other elements such as calcium, phosphorus and magnesium showed relatively low peaks. Equally, the results show that no elemental sulphur was recorded to have occurred within the constituents of the refined chitosan from shrimp shell wastes. This is most likely due to the chemical treatment of the precursor. The EDS compositional analysis results obtained on spectrum showed that the extracted chitosan contained 45.5, 25.2, 1.2, 15.7 and 7.0 wt% of O_2, C, P, Ca and Mg respectively.

Figures 16(a) and (b) show the respective BSED image of the extracted raw chitosan from shrimp shell wastes with the compositional testing point (spectrum) and the corresponding Energy Dispersive X-ray spectroscopy (EDS) pattern of testing point, spectrum. The corresponding EDS spectrum is shown in Figure 16(b), which reveals that the extracted raw chitosan from shrimp shell wastes indeed contains calcium, oxygen, magnesium, carbon and phosphorus. It can also be seen that oxygen and carbon showed the highest peaks in the EDS spectrum while elements such as calcium, magnesium and phosphorus showed relatively very low peaks thereby signifying their minute amounts present in the composition of the raw chitosan from shrimp shell wastes. The EDS plot in Figure 16(b) also corroborates the fact that no elemental sulphur was recorded and observed in the sample, signifying that the chemical processes of demineralization, deproteinization, and deacetylation were effective and efficient. The Energy Dispersive X-ray spectroscopy (EDS) compositional analysis of the raw chitosan (spectrum) show that the

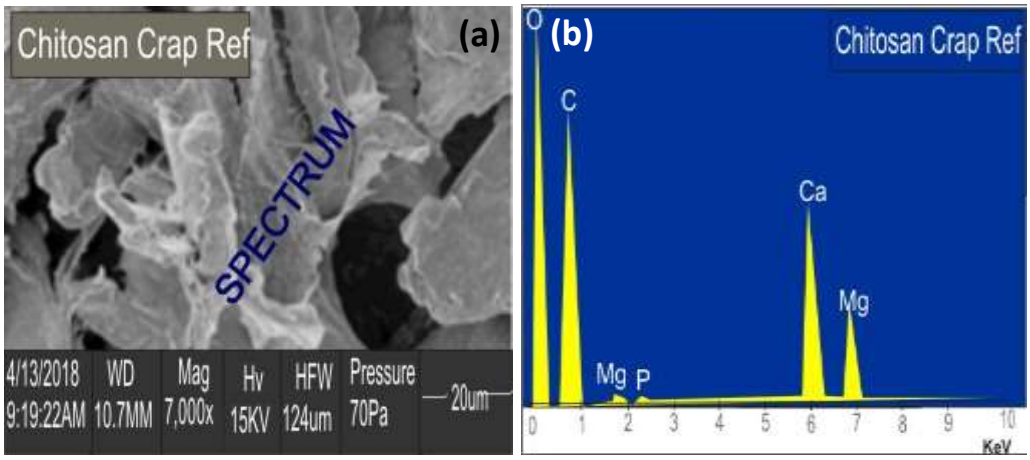

Figure 17. (a) BSED image of the refined chitosan from crab shell precursor showing the spectrum in which EDS analysis was carried out and (b) the corresponding EDS spectrum at the specified spectrum point as indicated in (a).

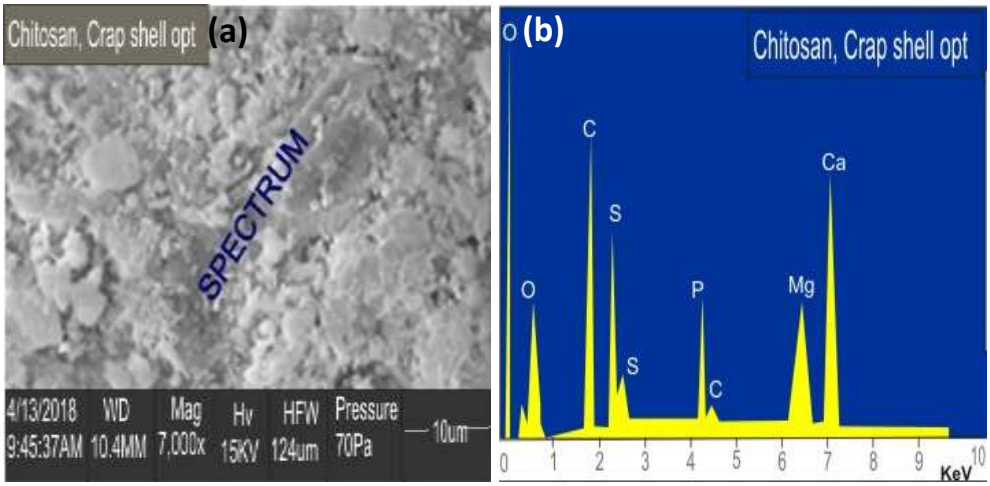

Figure 18. (a) BSED image of the raw chitosan from crab shell precursor showing the spectrum in which EDS analysis was carried out and (b) the corresponding EDS spectrum at the specified spectrum point as indicated in (a).

extracted biosorbent contains 44.0, 12.5, 7.2, 35.5 and 1.4 wt% of O_2, Ca, Mg, C and P respectively in its total composition.

The compositional analysis of the refined chitosan from shrimp shell wastes is shown in the BSED image in Figure 17(a), where the analysis was carried out on a specific area (spectrum) around the sample. The corresponding EDS spectrum plot is corroborated by Figure 17(b). The EDS spectrum pattern shows that oxygen peaks at 0.26 keV; carbon peaks at 0.85 keV; magnesium peaks at 1.9 keV and 7.0 keV; phosphorus peaks at 2.2 keV; and calcium peaks at 6.0 keV. Figure 17(b) shows that the extracted refined chitosan biosorbent from crab shell wastes contains C, Ca and O_2. Additionally, carbon and oxygen exhibited the highest peaks in the EDS spectrum while the other elements such as calcium, phosphorus and magnesium showed relatively low peaks. Furthermore, the results also show that no elemental sulphur was recorded to have occurred within the constituents of the refined chitosan from crab shell wastes owing to the chemical treatments of the precursor. The EDS compositional analysis obtained on spectrum showed that the extracted chitosan contained 40.5, 35.0, 1.2, 15.5 and 7.2 wt% of carbon, oxygen, phosphorus, calcium and magnesium respectively.

The extracted raw chitosan from crab shell precursor was also characterized using the Energy Dispersive X-ray spectroscopy (EDS). Figures 18(a) and (b) show the

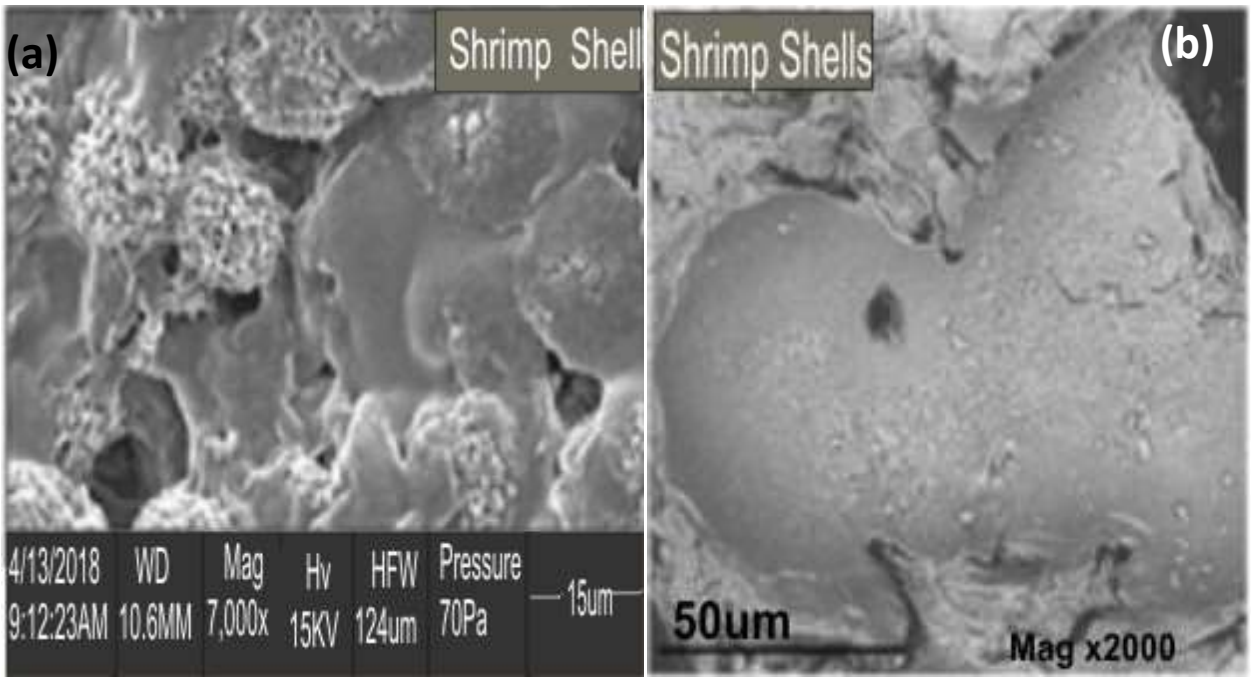

Figure 19. Microscopy images of pink shrimp shells precursor particles showing (a) SEM image at 7000X and (b) TEM image at 2000X.

respective BSED image of the raw chitosan biosorbent from crab shell wastes with compositional testing points (spectrum) and the corresponding Energy Dispersive X-ray spectroscopy (EDS) pattern of testing point, spectrum. The EDS plot in Figure 17(b) confirms that the extracted raw chitosan from crab shell wastes contains sulphur, oxygen, carbon, calcium, magnesium, and phosphorus. It can also be seen that calcium and carbon showed the highest peaks in the EDS spectrum at 7.0 and 1.82 keV respectively while the elements such as sulphur, oxygen, phosphorus and magnesium showed relatively very low peaks, signifying their minute amounts present in the composition of the raw chitosan from crab shell wastes. The EDS compositional analysis obtained on the spectrum showed that the extracted raw chitosan contained 10.0 wt% of sulphur, 10.4 wt% of oxygen, 26.0 wt% of carbon, 49.0 wt% of calcium, 10.4 wt% of phosphorus and 4.8 wt% of magnesium.

Surface morphology

A study of the surface morphology of the precursors and their respective extracted biosorbents was investigated using the Jeol JSM-7600F Field Emission Scanning Electron Microscope. This study was done to analyse the grain structure and roughness of the extracted biosorbents. The surface morphology of the shrimp shell precursor particles was studied by Scanning Electron Microscopy (SEM) and Transmission Electron Microscopy (TEM) and the corresponding micrographs at different magnifications and areas are shown in Figures19(a) and (b) respectively. Figure 19(a) shows the morphology of the shrimp shell wastes at higher magnification (×7000) in this study. The SEM micrograph shows that the structure of the shrimp shell waste is roughly spherical, approximately smooth, and grainy. The TEM image at a magnification of (×2000) confirmed these properties and also shows that the shrimp shell wastes precursor has some already existing pores with some rough edges within its structure.

Figures 20(a) and (b) shows the respective SEM micrograph of the crab shell particles at a magnification of (×7000) and the TEM image of the crab shell precursor at (×2000). The SEM micrograph shows that the structure of the crab shell wastes is rough, flat, uneven, coarse and grainy. The TEM image at a magnification of (×2000) shows that the scanned particles have little or no pores at least at a point/area of testing. It also confirms that the particles are rougher and coarser than the particles of the shrimp shell waste in Figures 19(a) and (b).

The extracted chitin particles from shrimp shell wastes were characterized using the Scanning Electron Microscope for its morphology and composition. The SEM image of the extracted chitin biosorbent particles at a magnification of (×7000) is shown in Figure 21(a) while the TEM micrograph of the biosorbent at a magnification of (×2000) is shown in Figure 21(b). The SEM micrograph of the chitin particles shows and confirms the change in the morphology of the converted shell wastes. It shows a

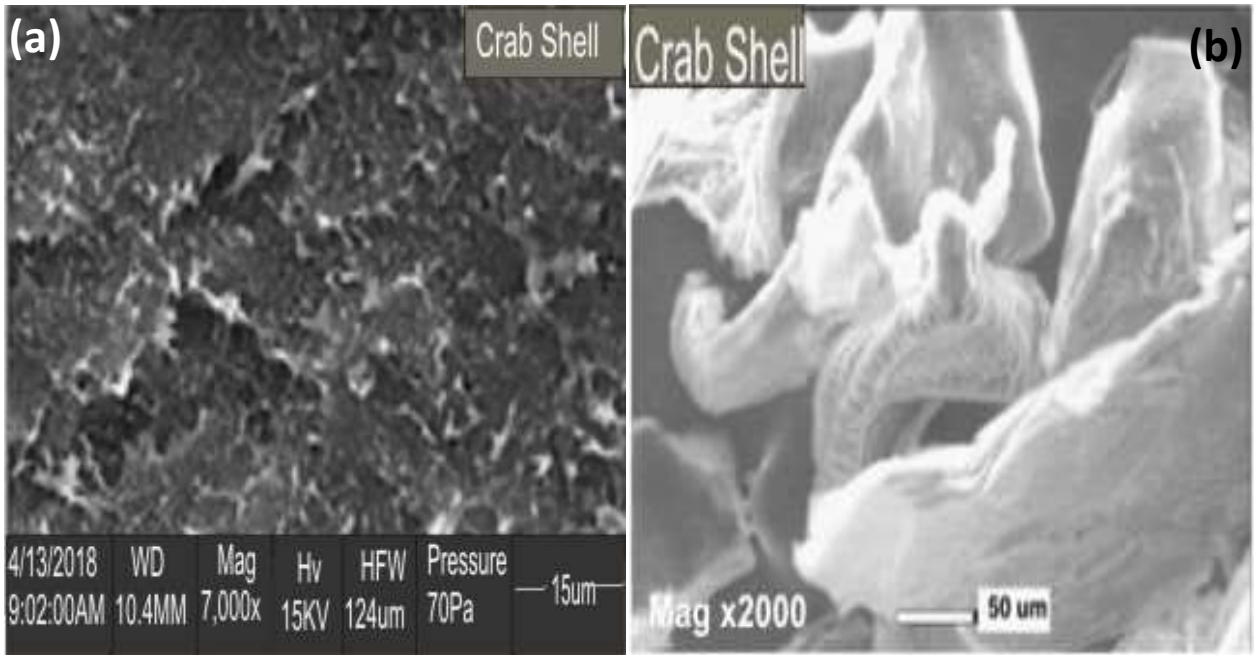

Figure 20. Microscopy images of crab shells precursor particles showing (a) SEM image at 7000X and (b) TEM image at 2000X.

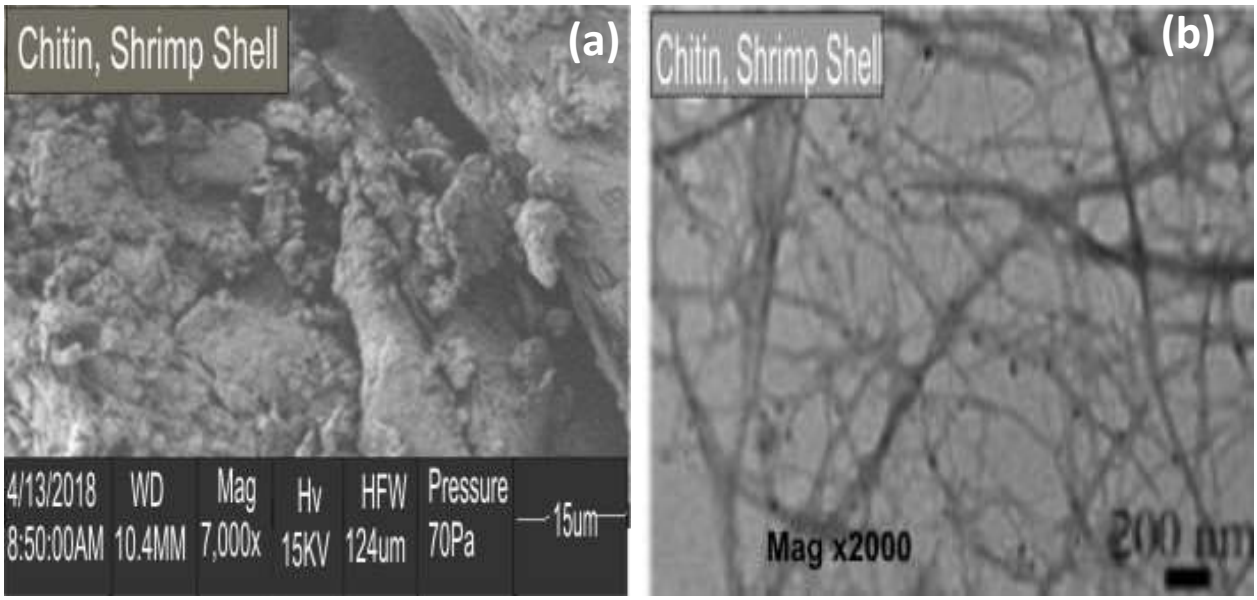

Figure 21. Microscopy images of chitin particles extracted from pink shrimp shell wastes showing (a) SEM image at 7000X and (b) TEM image at 2000X.

rougher surface and a significant increase in the porosity of the sample. The SEM image shows the presence of pores and fibers in the microstructure of the chitin particles from shrimp shell wastes. The TEM image in Figure 21(b) validates the structural attribute and feature of the extracted chitin. Here, the morphological study of the chitin particles invariably showed that the chemical process of extracting chitin from the shrimp shell wastes changed the structural characteristics of the precursor.

Figure 22(a) shows the Scanning Electron Microscopy in Z-contrast (compositional) mode (SEM image) of the extracted chitin particles from crab shell wastes at a

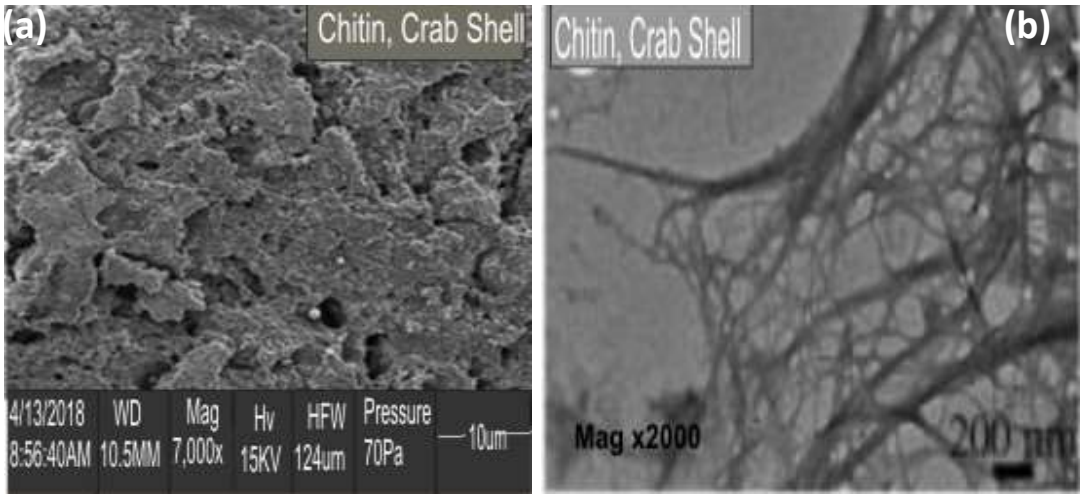

Figure 22. Microscopy images of chitin particles extracted from crab shells showing (a) SEM image at 7000X and (b) TEM image at 2000X.

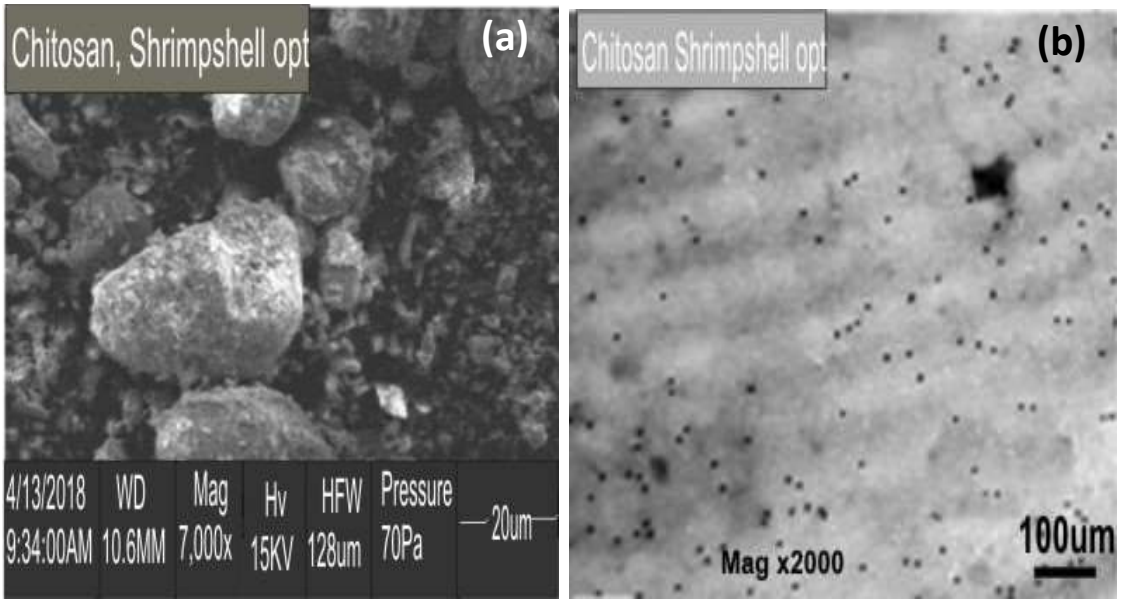

Figure 23. Microscopy images of raw chitosan particles extracted from pink shrimp shell wastes showing (a) SEM image at 7000X and (b) TEM image at 2000X.

magnification of (×7000) while the TEM micrograph of the extracted chitin at a magnification of (×2000) is shown in Figure 22(b). The SEM image of the chitin particles shows and confirms the morphological change of the converted crab shell wastes. It shows a rougher and grainier surface with a significant increase in the number of pores of the sample. The TEM image then shows the presence of pores and a highly connected fiber-like feature in the microstructure of the chitin particles from crab shell wastes. The TEM micrograph in Figure 22(b) validates the structural attribute and feature of the extracted chitin. Furthermore, the morphological study of the chitin particles invariably showed that the optimized chemical process of extracting chitin from the crab shell wastes changed the structural and physicochemical characteristics of the precursor.

The surface morphology of the extracted raw chitosan from shrimp shell precursor particles was studied by Scanning Electron Microscopy (SEM) and Transmission Electron Microscopy (TEM) and the corresponding micrographs at different magnifications and different areas are shown in Figure 23(a) and (b) respectively.

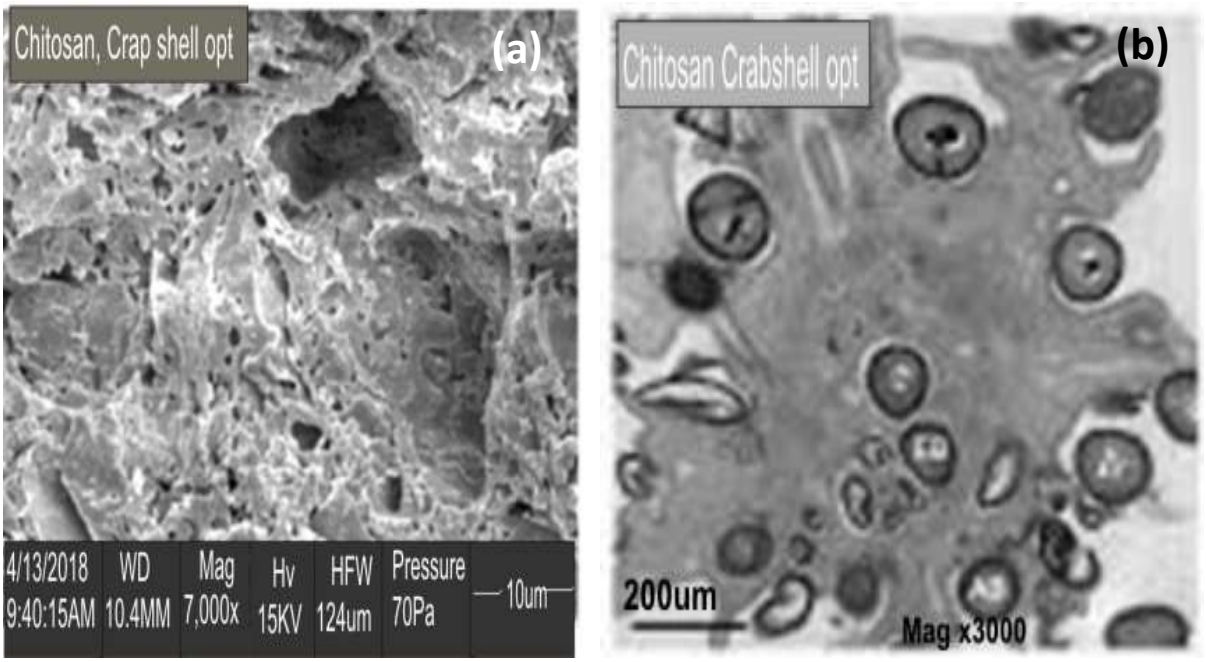

Figure 24. Microscopy images of raw chitosan particles extracted from crab shells showing (a) SEM image at 7000X and (b) TEM image at 3000X.

Figure 23(a) shows the morphology of the shrimp shells at higher magnification (×7000) in this study. The SEM micrograph shows that the structure of the extracted raw chitosan from shrimp shell wastes is roughly and almost spherical, rough, coarse and highly grainy. The TEM image at a magnification of (×2000) showed that the produced chitosan from shrimp shells precursor has a highly porous structure as indicated by the dark dots across the micrograph in Figure 23(b) with some rough edges within its structure.

Figures 24(a) and (b) show the respective Scanning Electron Microscopy in Z-contrast (compositional) mode (SEM image) and TEM micrograph of the extracted raw chitosan particles from crab shell wastes at a magnification of (×7000) and (×3000). The SEM image of the chitosan particles shows and confirms the morphological change of the converted crab shell wastes. It shows a rougher, grainier surface with a significant increase in the porosity of the sample (raw chitosan from crab shell wastes), from macropores to micropores. The TEM image then confirms the presence of an ample number of pores and the proximity to themselves along the microstructure of the raw chitosan particles from crab shell wastes. The TEM micrograph in Figure 24(b) authenticates the structural attribute and feature of the extracted chitosan. Furthermore, the morphological study of the chitosan particles revealed that the optimized chemical processes of the extraction of raw chitosan from the crab shell wastes changed the structural and physicochemical characteristics of the shell wastes efficiently.

The SEM image of the extracted refined (decolorized) chitosan particles from shrimp shell wastes at a magnification of (×7000) is shown in Figure 25(a) while its TEM micrograph at a magnification of (×2000) is shown in Figure 25(b). The SEM micrograph of the refined chitosan particles shows and confirms the change in the morphology and structure of the converted shell wastes. It shows a highly rough, grainy surface and a high number of pores that can be observed across the scanned area of the sample. The SEM image shows the presence of pores and uneven surface in the microstructure of the chitosan particles from shrimp shell wastes. The TEM image in Figure 25(b) validates the structural features of the extracted chitosan. This morphological study shows the efficiency of the optimized chemical processes in extracting refined chitosan from shrimp shell wastes.

The SEM image of the extracted refined chitosan particles at a magnification of (×7000) is shown in Figure 26(a) while its TEM micrograph at a magnification of (×2000) is shown in Figure 26(b). The SEM micrograph of the chitosan particles shows that the morphology of the converted shell wastes changed. It shows an extremely rough surface and a substantial increase in the porosity of the sample. The SEM image shows the presence of pores and the spherical nature the microstructure of the chitosan particles from crab shell wastes. The TEM image in Figure 26(b) validates the structural attribute and feature of the extracted refined chitosan, indicating a

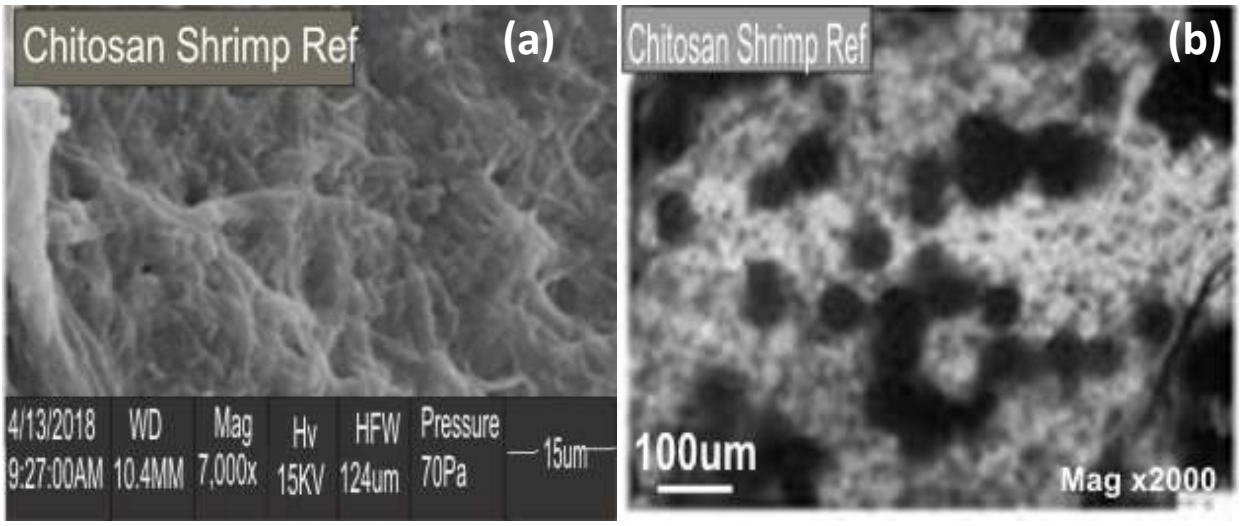

Figure 25. Microscopy images of refined chitosan particles extracted from pink shrimp shell wastes showing (a) SEM) image at 7000X and (b) TEM image at 2000X.

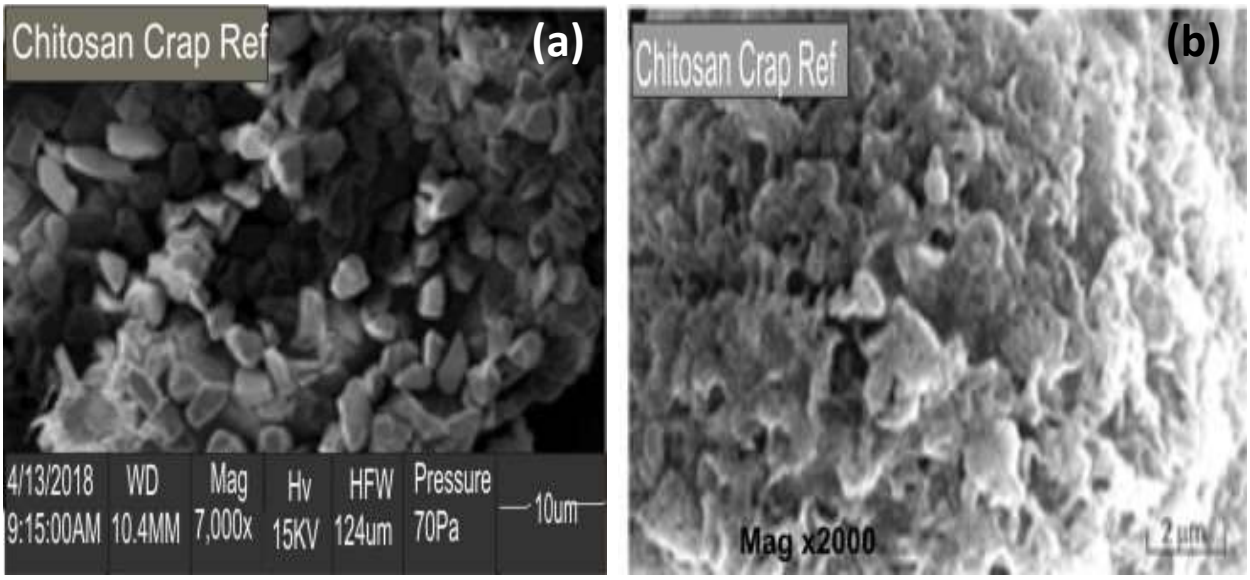

Figure 26. Microscopy images of refined chitosan particles extracted from crab shell wastes showing (a) SEM image at 7000X and (b) TEM image at 2000X.

highly grainy surface with significant number of pores. In this study, it can be inferred that due to the increase in the number of pores, the surface area of the biosorbent was also affected positively as observed in the BET surface area analysis.

Pore size distribution

The pore size and pore size distribution play a critical role in the application of materials in adsorption processes. Figure 27 displays the pore size and pore size distribution of the shrimp and crab shells precursor. In Figure 27(a), the pore size of the shrimp shell particles was in the range of < 20 and 350 µm, with 80% of the pores being concentrated between 40 and 350 µm. In Figure 27(b), the pore size of the crab shell particles is almost evenly distributed across the diameter range (< 20 – 350 µm) of the pore size distribution frequency plot.

The pore size and pore size distribution of optimized chitin particles extracted from shrimp shells and crab shells precursors are presented in Figure 28. In Figure

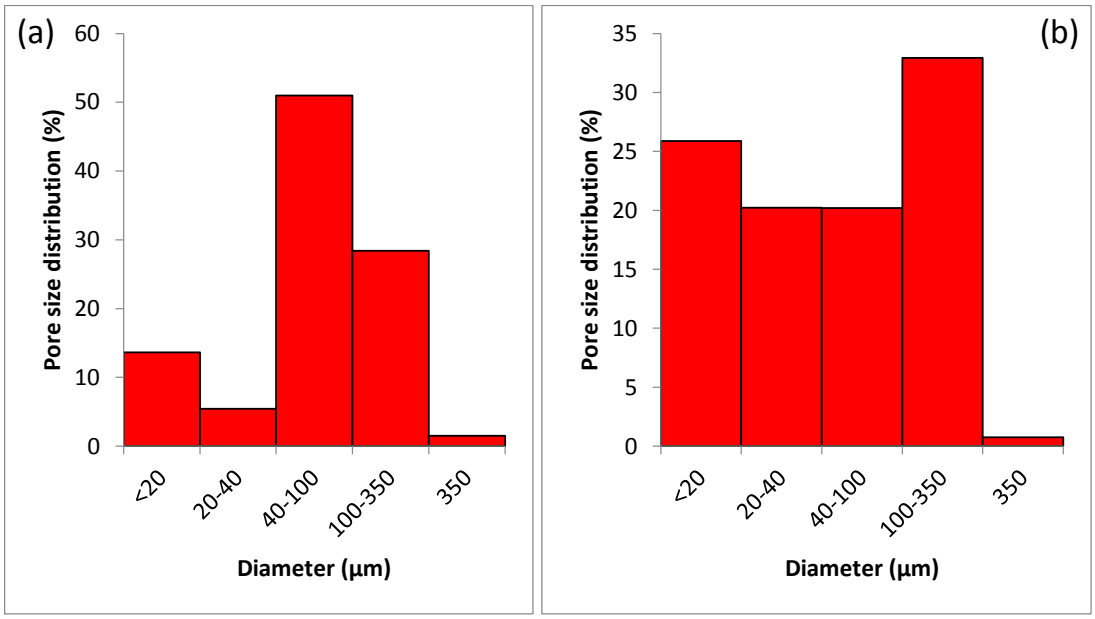

Figure 27. Pore size distribution of (a) pink shrimp shells precursor and (b) crab shells precursor.

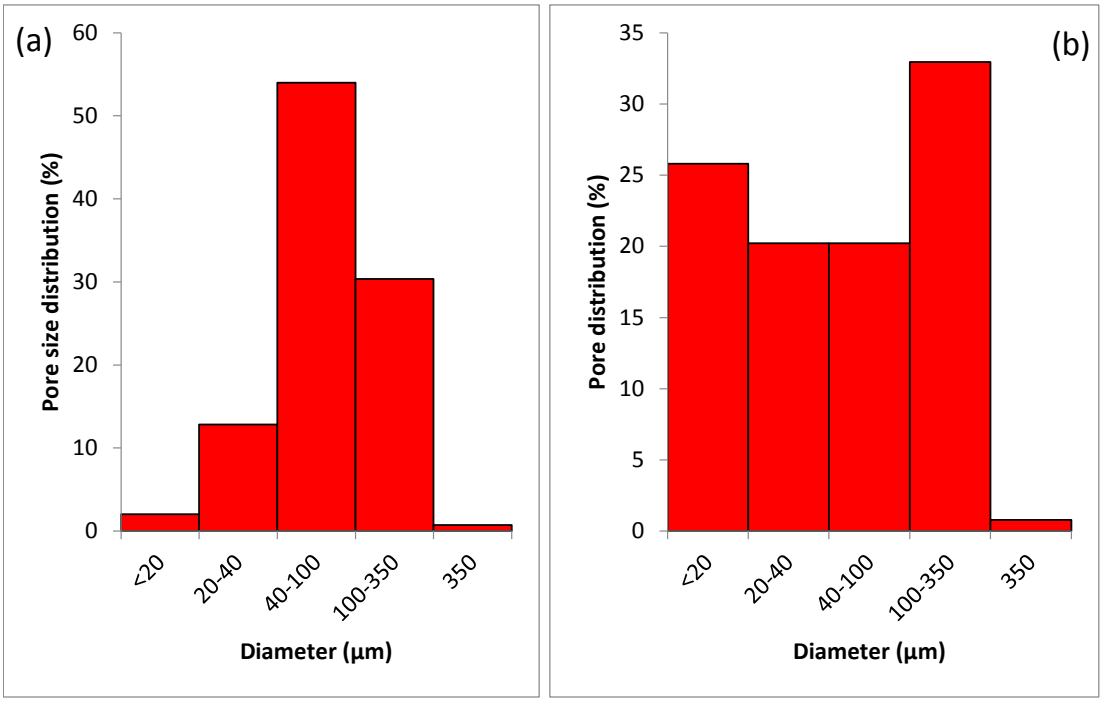

Figure 28. Pore size distribution of optimized chitin particles extracted from (a) pink shrimp shells precursor and (b) crab shells precursor.

28(a), the pore size distribution frequency revealed that about 70% of the pore sizes of the extracted optimized chitin particles are in-between the 40-100 µm diameter range. As shown in Figure 28(b), the distribution frequency of the pores in the extracted optimized chitin particles from crab shell wastes is virtually uniformly

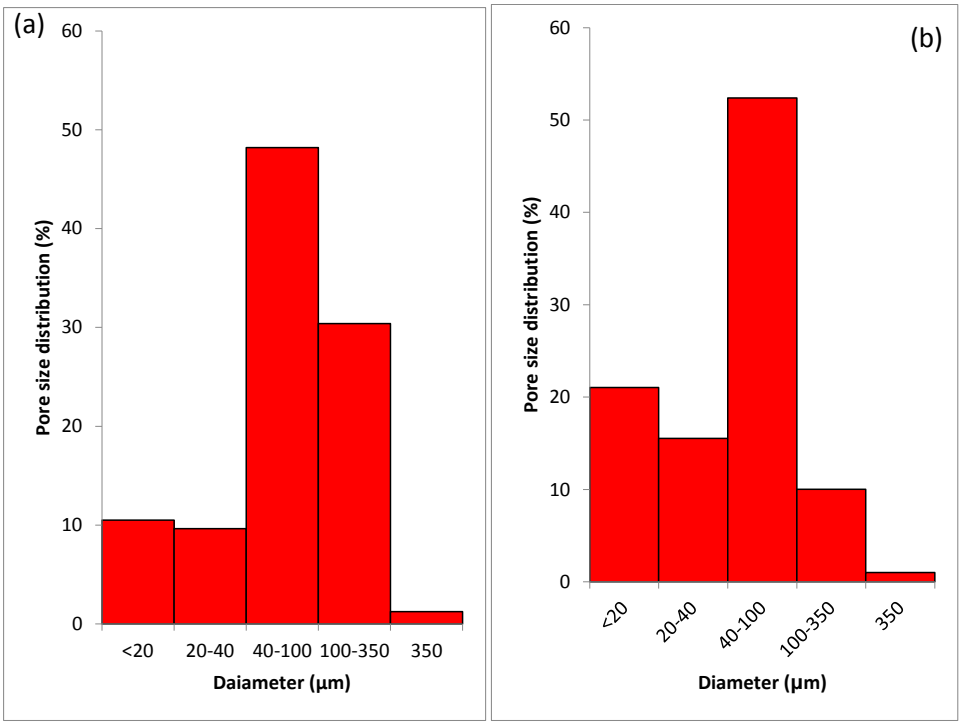

Figure 29. Pore size distribution of optimized refined chitosan particles extracted from (a) pink shrimp shells precursor and (b) crab shells precursor.

distributed across the (< 20 – 350 µm) diameter range of the distribution frequency chart. The average pore size diameters of the extracted chitin from the shrimp and crab shell wastes were obtained as 32.17 and 18.9 µm respectively.

Figure 29 displays the pore size and pore size distribution of the optimized refined chitosan particles extracted from shrimp and crab shell wastes. The pore size distribution frequency of the extracted chitosan particles from shrimp shell wastes, as depicted in Figure 29(a), shows that approximately 75% of the pore sizes fall in-between the 40-350 µm diameter range. The distribution frequency of the pores in the extracted optimized chitosan particles from crab shell wastes, as depicted in Figure 29(b), reveals that about 80% of the pore sizes fall into the (< 20-350 µm) range of the distribution frequency chart. The minimum pore size diameters of the extracted chitosan from the crab and shrimp shell wastes were obtained as 3.0 and 2.5 µm respectively while the maximum value was obtained as 350 µm each.

Conclusion

The processes of extraction of chitin from pink shrimp (*P. notialis*) and Lagoon crab (*C. amnicola*) shell wastes at optimized conditions through the chemical processes of demineralization, deproteinization and decolorization were investigated. The optimized conditions of producing raw and refined (optimized) chitin from crab and pink shrimp shells were obtained as (3.25 M HCl aqueous solution, period of demineralization of 18.55 h, 2.39 M NaOH aqueous solution and period of deproteinization of 2 h) and 3.25 M HCl aqueous solution, a demineralization time of 19.03 h, 2.43 M of NaOH aqueous solution and a deproteinization time of 2.03 h) respectively. The modelled optimized conditions for producing chitosan from chitin obtained from crab and pink shrimp shells were obtained as (50% w/w NaOH aqueous solution, temperature of 85.05°C and time of deacetylation of 133.64 min) and (50% w/w NaOH aqueous solution, deacetylation temperature of 87.9°C and time of 145.26 min) respectively. The modeled optimization conditions for the extraction process of the derived polymer that modeled the highest *DDA* of chitosan produced from crab and pink shrimp shell waste were (50% w/w NaOH aqueous solution, temperature of 84.46°C and time of deacetylation of 187 min) and (50% w/w NaOH aqueous solution, temperature of 87.9 ^{o}C and time of deacetylation of 90 min) respectively. The optimum yields of chitin from crab and pink shrimp shells were obtained as 19.36 and 26.08%, the optimum yields of chitosan from chitin obtained from crab and pink shrimp shell were 13.29 and 16.93% and their respective optimum *DDA* values of 84.2 and 89.73%. The values of the degree of deacetylation of the extracted chitosan determined by the FTIR and acid-base titration method were in the range of (81.32 and

82.25 %) and (82.15 and 89.73) respectively, which were within the commercial range of 30 - 95%. The physicochemical properties of the raw precursors and the extracted products were evaluated. Comprehensive characterization tests of all the materials under investigation (through BET surface area, FTIR, XRD, CrI, SEM, STEM and EDS) were carried out. Excellent agreements were achieved between the experimental FTIR bands of the refined chitosan from shrimp and crab shell wastes and the standard from Sigma Aldrich, Germany.

CONFLICT OF INTERESTS

The authors have not declared any conflict of interests.

REFERENCES

Abdou ES, Nagy KSA, Elsabee MZ (2008). Extraction and characterization of chitin and chitosan from local sources. Bioresource Technology 99:1359-1367.

Abubakar M, Alechenu AA, Manase A, Mohammed JA (2012). Comparative analysis and characterization of animal bones as adsorbent. Advances in Applied Science Research 3(5):3089-3096.

Ahmeda M, Marshall WE, Rao RM (1997). Potential of agricultural by-product based activated carbon for use in raw sugar decolourisation. Journal of Science, Food and Agriculture 75:117-124.

Akyeampong E (1999). Plantain production, marketing and consumption in west and central Africa. In Proceeding of International Symposium on banana and food security. Duala, Cameroon.

Al-Sagheer FA, Al-Sughayer MA, Muslim S, Elsabee MZ (2009). Extraction and characterization of chitin and chitosan from marine sources in Arabian Gulf. Carbohydrate Polymers 77:410-419.

Al-Shahrani H, Alakhras F, Al-Abbad E, AL-Mazaideh G, Hosseini-Bandegharaei A, Ouerfelli N (2018). Sorption of cobalt (II) ions from aqueous solutions using chemically modified chitosan. Global NEST Journal 20(3):620-627.

Ambarish CN, Sridha KR (2015). Isolation and characterization of chitin from exoskeleton of pill-millipedes. Trends in Biomaterilas and Artificial Organs 29:155-159.

Amoo KO, Olafadehan OA, Ajayi TO (2019). Optimization studies of chitin and chitosan production from Penaeus notialis shell waste. African Journal of Biotechnology 18:670-688.

Amos TT (2007). Production and productivity of crustacean in Nigeria. Journal of Social Sciences 15(3):229-233.

Association of Official Analytical Chemists (AOAC) (1990). Official methods of analysis. Washington DC.

Aranaz I, Mengibar M, Harris R, Panos I, Miralles B, Acosta N, Heras A (2009). Functional characterization of chitin and chitosan. Current Chemical Biology 3(2):203-230.

Arbia W, Adour L, Amrane A, Lounici H (2013). Optimization of medium composition for enhanced chitin extraction from Parapenaeus longirostris by Lactobacillus helveticus using response surface methodology. Food Hydrocolloids 31(2):392-403.

ASTM-D-4607 (1994). Standard test method for determination of iodine number of activated carbon. West Conshohocken, Philadelphia, United States: American Society for Testing and Materials (ASTM) International (Reapproved 2011).

Campana-Fillio SP, De Britto D, Curti E, Abreu FR, Cardoso MB, Battisti MV, Sim PC, Lavall RL (2007). Extraction, structures and properties of α- and β-chitin. Quim Nova 30(3):644-650.

Casadidio C, Peregrina D V, Gigliobianco MR, Deng S, Censi R, Di Martino P (2019). Chitin and chitosans: Characteristics, eco-Friendly processes, and applications in cosmetic science. Marine Drugs 17(6):369.

Cho YI, No HK, Meyers SP (1998). Physicochemical characteristics and functional properties of various commercial chitin and chitosan products. Journal of Agriculture and Food Chemistry 46(9):3839-3843.

Crews P, Rodriguez J, Jaspars M (2009). Organic Structure Analysis. 2nd Edition, Oxford University Press, New York.

Daraghmeh NH, Chowdhry BZ, Leharne SA, Al Omari MM, Badwan AA (2011). Chitin. Profiles of Drug Substances, Excipients, and Related Methodology 36:35-102.

EUCHIS (2017). 13th International Conference of the European Chitin Society Conference, 8th SIAQ.

Fan Y, Saito T (2009). Nano-fibrillation of chitins by TEMPO-mediated oxidation or protonation of amino groups. Functional Materilas 29:19-24.

Fan Y, Saito T, Isogai A (2008). Chitin nanocrystals prepared by TEMPO-mediated oxidation of alpha chitin. Biomacromolecules 9(1):192-198.

Food and Agriculture Organization of the United Nations (FAO) (2017). The future of food and agriculture – Trends and challenges. Rome.

Galed G, Diaz E, Goycoolea FM, Heras A (2008). Influence of N-deacetylation on chitosan production from alpha chitin. National Product Communication 3(4):543-550.

Ghimire S, Neupane B, Pokhrel S, Le HH, Lebek W, Heinrich G, Adhikari R (2011). Conversion of chitin isolated from fresh-water prawns to chitosan and its characterization. Polymers Research Journal 11(1):1-15.

Hajji S, Younes I, Ghorbel-Bellaaja O, Hajji R, Rinaudo M, Nasri M, Jellouli K (2014). Structural differences between chitin and chitosan extracted from three different marine sources. International Journal of Biological Macromolecules 65:298-306.

Hayes M, Carney B, Slater J, Brück W (2008). Mining marine shellfish wastes for bioactive molecules: Chitin and chitosan -Part A: Extraction methods. Biotechnology Journal 3(7):871-877.

Huthman AS, Buhari F, Olagunju J, Odawn A, Huthman OI (2013). Chemical analysis and characterization of shrimp chitosan in shrimp shell waste from Lagos lagoon, Nigeria. International Journal of Chemical and Pharmaceutical Research 2(11):377-385.

Ibitoye EB, Lokman IH, Hezmee MN, Goh YM, Zuki ABZ, Jimoh AA (2018). Extraction and physicochemical characterization of chitin and chitosan isolated from house cricket. Biomedical Materials 13:1-12.

Ifuku S, Nogi, M, Abe K, Yoshioka M, Morimoto M, Saimoto H, Yano H (2009). Preparation of chitin nanofibers with a uniform width as α-chitin from crab shells. Biomacromolecules 10:1584-1588.

Isa MT, Ameh AO, Gabriel JO, Adama KK (2012). Extraction and characterization of chitin from Nigerian sources. Leonardo Electronic Journal of Practices and Technologies 21:73-81.

Jang MK, Kong BG, Jeong YI, Lee CH, Nah JW (2014). Physicochemical characterization of α-chitin, β-chitin, and γ-chitin separated from natural resources. Journal of Polymer Science Part A: Polymer Chemistry 42:3423-3432.

Jayakumar RP, Chandrasekaran V (2014). Adsorption of lead (II) ions by activated carbons prepared from marine green algae: equilibrium and kinetics studies. International Journal of Industrial Chemistry 5(10):1-9.

Ji Y, Wolf PS, Rodriguez IA, Bowlin GL (2012). Preparation of chitin nanofibril/polycaprolactone nanocomposite from a nonaqueous medium suspension. Carbohydrate Polymers 87:2313-1319.

Jones RT, Pawlik C (2019). Coballt recovery from South African copper smelters. Proceedings of the 58th Annual Conference of metallurgists (COM) hosting the 10th international copper conference, Copper 2019 1-8.

Kaya M, Baran T, Mentes A, Asaroglu M, Sezen G, Tozak KO (2014). Extraction and characterization of α-chitin and chitosan from six different aquatic invertebrates. Biophysics 9:145-157.

Kaya M, Erdogan S, Mol A, Baran T (2015). Comparison of chitin structures isolated from seven orthoptera species. International Journal of Biological Macromolecules 72:797-805.

KFDA (1995). Korea Food Additive Code (KFDA). Seoul, Korea Republic.

Khan AA, Muthukrishnan M, Guha BK (2009). Sorption and transport modeling of hexavalent chromium on soil media. Journal of Hazardous Materials 54:444-454.

Kim JW, Sohn MH, Kim DS, Sohn SM, Kwon YS (2001). Production of granular activated carbon from waste walnut shell and its adsorption characteristics for Cu^{2+} ion. Journal of Hazardous Materials B85:301-315.

Knorr D (1984). Use of chitinous polymers in food – A challenge for food research and development. Food Technology 38(1):85-97.

Kumirska J, Czerwicka M, Kaczyński Z, Anna Bychowska A, Brzozowski K, Thöming J, Stepnowski P (2010). Application of spectroscopic methods for structural analysis of chitin and chitosan. Marine Drugs 8(5):1567-1636.

Li Q, Dunn ET, Grandmaison EW, Goosen MFA (1992). Applications and properties of chitosan. Journal of Bioactive and Compatible Polymers 7:370-397.

Limam Z, Selmi S, Sadok S, El Abed A (2011). Extraction and characterization of chitin and chitosan from crustacean by-products: Biological and physiochemical properties. African Journal of Biotechnology 10(4):640-647.

Liu S, Sun J, Yu L, Zhang C, Bi J, Zhu F, Yang Q (2012). Extraction and characterization of chitin from the beetle Holotrichia parallela Motschulsky. Molecules 17:4604-4611.

Majitán J, Bíliková K, Markovič O, Gróf J, Kogan G, Šimúth J (2007). Isolation and characterization of chitin from bumblebee (Bombus terrestris). International Journal of Biological Macromolecules 40:237-241.

Mohanasrinivasan V, Mishra M, Paliwal J, Singh S, Selvarajan E, Suganthi V (2014). Studies on heavy metal removal efficiency and antibacterial activity of chitosan prepared from shrimp shell waste. 3 Biotech 4(2):167-175.

Morin-Crini N, Lichtfouse E, Torri G, Crini G (2019). Applications of chitosan in food, pharmaceuticals, medicine, cosmetics, agriculture, textiles, pulp and paper, biotechnology, and environmental chemistry. Environmental Chemistry Letters. https://doi.org/10.1007/s10311-019-00904-x

Muzzarelli RAA, Peter MG (1997). Chitin Handbook. Grottammare, Italy, European Chitin Society, Atec.

Nessa F, Shah Md. Masum, Asaduzzaman M, Roy SK, Hossain MM, Jahan MS (2010). A process for the preparation of chitin and chitosan from prawn shell waste. Bangladesh Journal of Scientific and Industrial Research 45(4):323-330.

Nithya A, Jothivenkatachalam K, Prabhu S, Jeganathan K (2014). Chitosan based nanocomposite materials as photocatayst (A review). Materials Science Forum 781:79-94.

No HK, Lee KS, Meyers SP (2000). Correlation between physicochemical characteristics and binding capacities of chitosan products. Journal of Food Science 65(7):1134-1137.

No HK, Meyers SP (1992). Utilization of crawfish processing wastes as carotenoids, chitin, and chitosan sources. Journal of the Korean Society of Food Science and Nutrition 21(3):319-326.

No HK, Meyers SP (1995). Preparation and characterization of chitin and chitosan-A Review. Journal of Aquatic Food Product Technology 4(2):27-52.

Noishiki Y, Takami H, Nishiyama Y, Wada M, Okada S, Kuga S (2003). Alkali-induced conversion of β-chitin to α-chitin. Biomacromolecules 4:896-899.

Nouri M, Khodaiyan F, Razavi HS, Mousavi M (2016). Improvement of chitosan production from Persian Gulf shrimp waste by response \surface methodology. Food Hydrocolloids 59:50-58.

Olafadehan OA, Ajayi TO, Amoo KO (2020). Optimum conditions for extraction of chitin and chitosan from *Callinectes amnicola* shell waste. Theoretical Foundations of Chemical Engineering 54:1173-1194.

Olafadehan OA, Jinadu OW, Salami L, Popoola LT (2012). Treatment of brewery wastewater effluent using activated carbon prepared from coconut shell. International Journal of Applied Science and Technology 2(1):165-178.

Prashanth R, Tharanathan R (2007). Chitin/chitosan: modifications and their unlimited application potentialan overview. Trends in Food Science and Technology 18:117-131.

Ravi Kumar MNV (2000). A review of chitin and chitosan applications. Reactive and Functional Polymers 46(1):1-27.

Rinaudo M (2006). Chitin and chitosan: Properties and application. Progress in Polymer Science 31:603-632.

Roberts GAF (1992). Chitin Chemistry. MacMillan, London, UK.

Roberts GAF (2007). The road is long. Advanced Chitin Science 10:3-10.

Sandford PA (1992). High purity chitosan and alginate: Preparation, analysis, and applications. Front Carbohydrate Research 2:250-269.

Sarbon NM, Sandanamsamy S, Kamaruzaman SFS, Ahmad (2014). Chitosan extracted from mud crab (Scylla olivicea) shells: physicochemical and antioxidant properties. Journal of Food Science and Technology 52(7):4266-4275.

Shirai K, Palella D, Castro Y, Guerrero-Legarreta I, Saucedo-Castaneda G, Huerta-Ochoa S, Hall GM (2003). Characterization of chitins from lactic acid fermentation of prawn wastes. In Advances in Chitin Science; Chen, R.H., Chen, H.C., Eds.; Elsevier: Taiwan, 1998 3:103-110.

Struszczyk MH (2002). Chitin and chitosan: Part I. properties and production. Polimery 47:316-325.

Sudha PN, Aisverya S, Gomathi T, Vijayalakshmi K, Saranya M, Sangeetha, K, Latha S, Sabu Thomas S (2017). Application of chitin/chitosan and its derivatives as adsorbents, coagulants, and flocculants. Chitosan pp. 453-487.

Synowiecki J, Al-Khateeb NA (2003). Production, properties, and some new applications of chitin and its derivatives. Critical Reviews in Food Science and Nutrition 43(2):145-171.

Tajik H, Moradi M, Rohani SMR, Erfani AM, Jalali FSS (2008). Preparation of chitosan from brine shrimp (Artemia urmiana) cyst shells and effects of different chemical processing sequences on the physicochemical and functional properties of the product. Molecules 13:1263-1274.

Walther HJ (1983). Carbon Adsorption Handbook. Edited by P. N. Cheremisinoff and F. Ellerbusch. Second Printing. USA, Michigan, Collingwood. Ann Arbor Science Publishers, 1980, 1054 S., 393 Abb. ISBN 0-250-40236-X. Acta Hydrochimica et Hydrobiologica 11:22–

Yildiz B, Sengul B, Ali G, Levent I, Seval BK, Soner C, Habil UK (2010). Chitin–chitosan yields of fresh water crab (Potamon potamios, Olivier 1804) shell. Pakistan Veterinary Journal 30(4):227-231.

Yousef RI, El-Eswed B (2009). The effect of pH on the adsorption of phenol and chlorophenols onto natural zeolite. Colloids and Surfaces A: Physicochemical and Engineering Aspects 334(1):92-99.

Zhang AJ, Qin QL, Zhang H, Wang HT, Li X, Miao L, Wu YJ (2011). Preparation and characterisation of food-grade chitosan from housefly Larvae. Czech Journal of Food Sciences 29(6):616-623.